Process compatible desulfurization of NSP cement production: A novel strategy for efficient capture of trace SO_2 and the industrial trial

Tongsheng Zhang[a,b], Hui Peng[a], Chang Wu[a], Yiqun Guo[a], Jiawei Wang[c], Xinzhi Chen[d], Jiangxiong Wei[a,b]✉, Qijun Yu[a,b,e]✉

[a] School of Materials Science and Engineering, South China University of Technology, 510640, Guangzhou, China

[b] Guangdong Low Carbon Technology and Engineering Center for Building Materials, 510640, Guangzhou, China

[c] Energy and Bioproducts Research Institute (EBRI), Aston University, Aston Triangle, B4 7ET Birmingham, UK

[d] Guangdong Wanyin Technology Development Co. Ltd, 510075, Guangzhou, China

[e] College of Civil Engineering, Hefei University of Technology, 230009, Hefei, China

Highlights

1. SO_2 capture by calcium-based adsorbents in the preheater environment was studied.
2. Higher SO_2 capture efficiency was obtained after introducing V_2O_5-based catalysts.
3. Catalyst-assisted SO_2 capture with de-SO_2 efficiency of 75.5% was first reported.
4. A novel process compatible FGD technology was proposed and designed.
5. SO_2 in flue gas reduced from 1080 mg/Nm^3 to <100 mg/Nm^3 during industrial trial.

Abstract

Cement industry contributes to more and more SO_2 emission due to utilization of alternative raw materials and fuels, whereas the available calcium-based dry flue gas desulfurization (FGD) technologies present low efficiency due to slow reversible de-

✉ Corresponding author. Email address: jxwei@scut.edu.cn. (Jiangxiong Wei). Tel.: +86-020-87114137.

✉ Corresponding author. Email address: concyuq@hfut.edu.cn. (Qijun Yu). Tel.: +86-020-87114233.

SO_2 reactions and short gas-solid contact time in the preheater. In the present study, the SO_2 capture potentials of $CaCO_3$, CaO, and $Ca(OH)_2$ in the preheater environment were maximized by introducing V_2O_5-based catalyst and selecting optimal reaction temperature, and the de-SO_2 mechanism was extensively discussed. The results showed that the de-SO_2 efficiency of calcium-based adsorbents increased by 10-57 times as SO_2 was effectively oxidized to SO_3 in the presence of V_2O_5-based catalyst, then maximum de-SO_2 efficiency of 75.5% was achieved using $Ca(OH)_2$ and V_2O_5-CeO_2 at 600 ºC. Furthermore, $CaCO_3$ assisted by V_2O_5-CeO_2 also had a de-SO_2 efficiency of 65.6%. Subsequently, a novel process compatible FGD technology was designed to maximize the de-SO_2 ability of raw meal in the preheater by adding V_2O_5-based catalyst and humidification, the SO_2 concentration of flue gas reduced from 1000 mg/Nm^3 to less than 100 mg/Nm^3 in the industrial-scale trial, as more sulfur was solidified into clinker in the form of alkali sulfate without reducing its properties. This novel process compatible de-SO_2 strategy is of real significance for reducing SO_2 emission of cement industry at low economic cost.

Keywords: Calcium-based adsorbents; Catalyst-assisted SO_2 capture; NSP cement production; Process compatible desulfurization; SO_2

1 Introduction

In the current cement industry, limestone ($CaCO_3$), clay ($Al_2O_3 \cdot xSiO_2 \cdot yH_2O$), ferreous material, and corrective constituents are used to prepare raw meal (Bullerjahn

et al., 2014; Shen et al., 2017; Shi et al., 2019), which consequently goes through milling, pre-heating, pre-calcination, melting, reaction, and rapid cooling (Gao et al., 2016; Ige et al., 2021). Then the clinker obtained, supplementary cementitious materials, and gypsum are further ground to prepare different types of Portland cement (Juenger et al., 2019; Peys et al., 2022; Snellings, 2016). To improve the production efficiency of clinker, the new suspension preheater (NSP) cement production process, as shown in **Fig. 1,** has been developed and widely applied since the 1980s. Since the pre-heating of raw meal and the decomposition of carbonates are achieved in separate preheater and pre-calciner rather than traditional rotary kiln, the energy efficiency is significantly improved (Liu et al., 1995; Xu et al., 2015). This benefits from the rapid heat transfer between hot gas and solid with contrary flow direction and direct heating for limestone decomposition in a suspension state (**Table 1**). Additionally, the production capacity of high-quality clinker is also significantly increased by rational arranging the temperature distribution of the whole NSP cement production process.

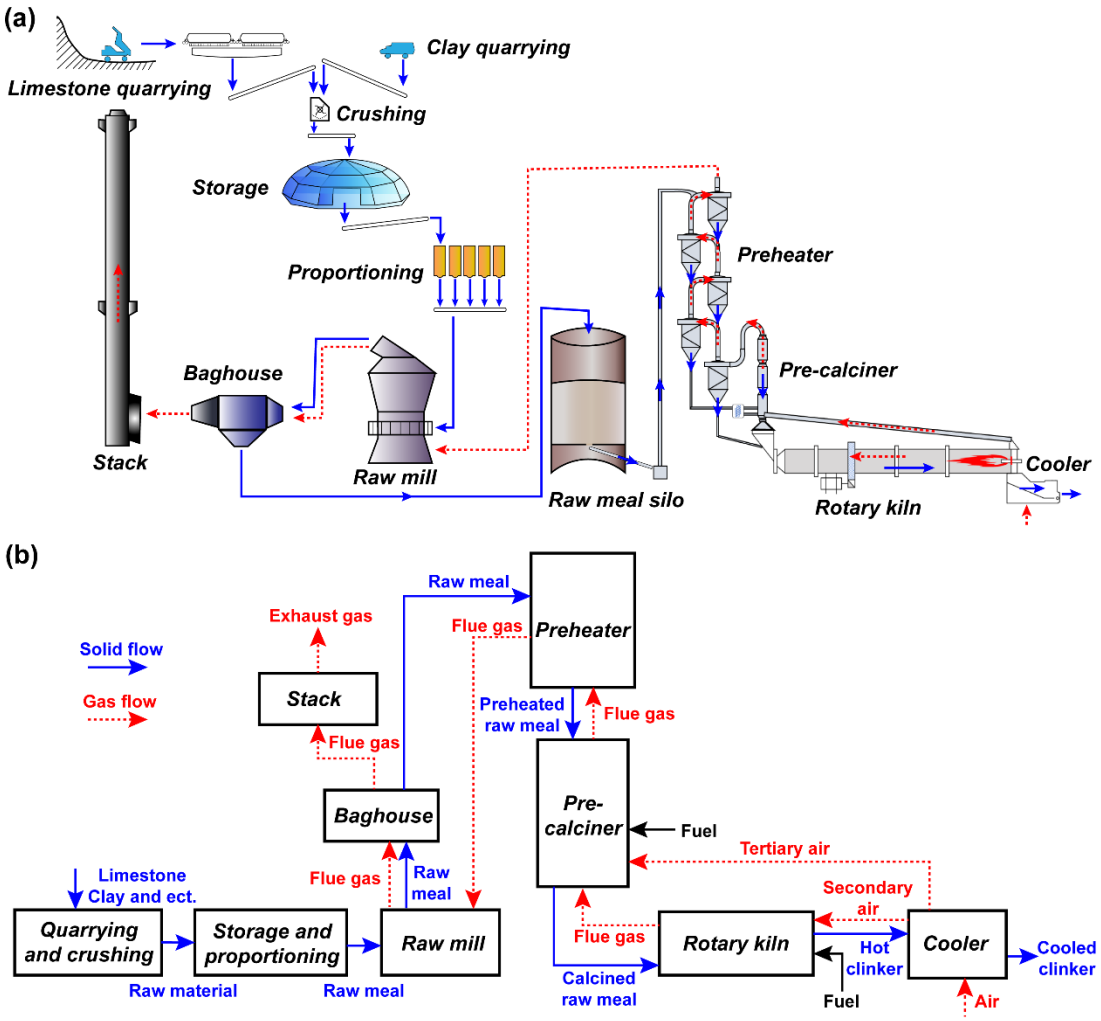

Fig. 1. The whole process of cement clinker production. (a) Schematic diagram; (b) Solid and gas flow (Zhang et al., 2019a).

Table 1

Physical and chemical changes of raw meal during NSP cement production process.

Equipment	Temperature	Process	Reaction equations
Raw mill	80-300 °C	Evaporation	$H_2O \rightarrow H_2O\uparrow$
Preheater	300-950 °C	Evaporation Dehydration of clay minerals Decomposition of partial carbonates	$H_2O \rightarrow H_2O\uparrow$ $Al_2O_3 \cdot 2SiO_2 \cdot 2H_2O \rightarrow Al_2O_3 \cdot 2SiO_2 + 2H_2O\uparrow$ $MgCO_3 \rightleftharpoons MgO + CO_2\uparrow$
Pre-calciner	900-1000 °C	Decomposition of carbonates	$MgCO_3 \rightleftharpoons MgO + CO_2\uparrow$ $CaCO_3 \rightleftharpoons CaO + CO_2\uparrow$
Rotary kiln	1000-1450 °C	Solid reaction Sintering of clinker	$2CaO + SiO_2 \rightarrow \beta\text{-}C_2S$ $3CaO + SiO_2 \rightarrow C_3S$ $\beta\text{-}C_2S + CaO \rightarrow C_3S$ $3CaO + Al_2O_3 \rightarrow C_3A$ $4CaO + Al_2O_3 + Fe_2O_3 \rightarrow C_4AF$
Clinker cooler	1000-300 °C	Cooling of clinker	—

With the awareness enhancement of environmental protection, more and more attention has been paid to the SO_2 emission from NSP cement production. Extensive studies (Hansen et al., 2003; Miller and Hansen, 2004; Mut et al., 2015; Rasmussen, 2012; Zhang et al., 2019a; Zhang et al., 2019b) have shown that about 80% SO_2 is attributed to the decomposition of sulfides (mainly pyrite, FeS_2) in the C2-C3 cyclone, and the rest SO_2 is released from the combustion of fuel and the decomposition of partial sulfates (mainly gypsum, $CaSO_4$) in the rotary kiln. On the other hand, SO_2 can be captured by several approaches as shown in **Fig. 2** as residual sulfate in the clinker and discharged from the kiln head with it (Zhang et al., 2019b). Specifically, SO_2 can react with alkali oxides during clinkerization in the kiln to form K_2SO_4, Na_2SO_4, and even $CaSO_4$, and most of SO_2 released in the kiln can be effectively captured by massive CaO in the pre-calciner and C5 cyclone. Thus, SO_2 released from fuel and sulfates cannot result in excessive SO_2 emission in the flue gas. However, only a small proportion of SO_2 can be captured by $CaCO_3$ when passing through the preheater and raw mill, resulting in relatively high SO_2 emission in the flue gas.

Theoretically, the reaction rate of SO_2 and $CaCO_3$ to form $CaSO_3$ is very slow, especially at high temperature and high CO_2 concentration environments (Czyzewski et al., 2013; I. Ávila et al., 2005; Rasmussen, 2012). Furthermore, most $CaSO_3$ decomposes easily and releases SO_2 again in the preheater, as the decomposition temperature of $CaSO_3$ is about 650 ^oC. Only a few of $CaSO_3$ can be oxidized to $CaSO_4$, which can be transferred into the kiln with raw meal. During clinkerization, most sulfur-

containing minerals in clinker are tend to decompose or volatilize as shown in **Table 2**. After numerous release-capture cycles of SO_2 as shown in **Fig. 2**, partial of sulfur is discharged with clinker in the form of $CaSO_4$, alkali sulfates, and trace $CaO{\cdot}3Al_2O_3{\cdot}CaSO_4$, otherwise the rest sulfur is emitted with flue gas in the form of SO_2. That is to say, although the NSP cement production system itself can capture SO_2, it is still difficult to meet the emission limits of SO_2 due to its extremely limited capture capacity.

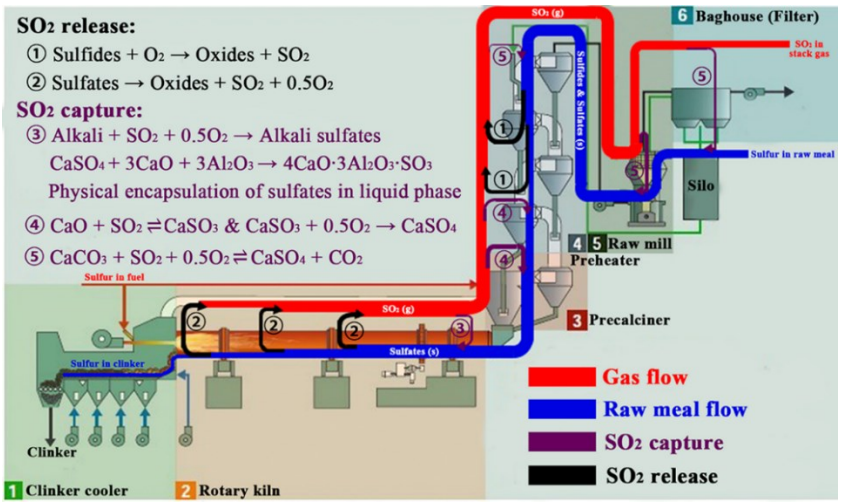

Fig. 2. Schematic sulfur flow, SO_2 release and capture in a typical NSP cement production system (Zhang et al., 2019b).

Table 2

Thermal stability of sulfur-containing phases in cement clinker.

Chemical formula	$CaSO_3$	$CaSO_4$	$4CaO{\cdot}2SiO_2{\cdot}CaSO_4$
Change	Decomposition or oxidation to $CaSO_4$	Partial decomposition	Complete decomposition
Reaction Temperature	650 °C	1300-1350 °C	~1200 °C
Content in clinker	Nil	Paucity	Nil

Chemical formula	K_2SO_4	$NaSO_4$	$CaO·3Al_2O_3·CaSO_4$
Change	Partial volatilization	Partial volatilization	Partial decomposition
Reaction Temperature	~1400 °C	~1300 °C	1350-1400 °C
Content in clinker	Trace	Trace	Trace

In order to reduce SO_2 emissions of the cement industry, wet flue gas desulfurization (WFGD) technologies, such as limestone-gypsum and dual alkali methods, are introduced for tail-end flue gas purification (Chen et al., 2021; Poullikkas, 2015). Although with outstanding desulfurization (de-SO_2) efficiency, wet FGD technologies present large investments, high energy and water consumption, and easy corrosion of equipment, resulting in high maintenance cost to be accepted by the actual cement industry.

To reduce de-SO_2 cost, process compatible de-SO_2 conception has been proposed to enhance SO_2 capture capability of the preheater section by injecting calcium-based adsorbents (Han et al., 2015; Przepiorski et al., 2013; Yu et al., 2020), meanwhile, the desulfurization product is combined into clinker without any liquid or solid wastes. For instance, partial hot raw meal (or external CaO) is injected into C1 cyclone to achieve a de-SO_2 efficiency of 30~40% (**Fig. 3a**), as CaO is much more reactive than $CaCO_3$. For advanced dry FGD technology (**Fig. 3b**), hot raw meal is preferentially slaked before injecting into C1 cyclone, external $Ca(OH)_2$ or carbide slag are also be used sometimes, which can achieve a maximum de-SO_2 efficiency of 50~60%. However, the

available dry FGD technologies have poor adaptability to SO_2 fluctuations in the flue gas, especially for high SO_2 concentrations. Recycling excessive hot raw meal (> 5%) leads to poor burnability and higher energy consumption. Even worse, decomposition of $CaSO_3$ (desulfurization product) cannot be avoided when the temperature surpasses 650 °C (Borgwardt, 1970; Bueno-Lopez and Garcia-Garcia, 2005), resulting in a much lower efficiency of available dry FGD technologies than that of wet FGD technologies (> 95%).

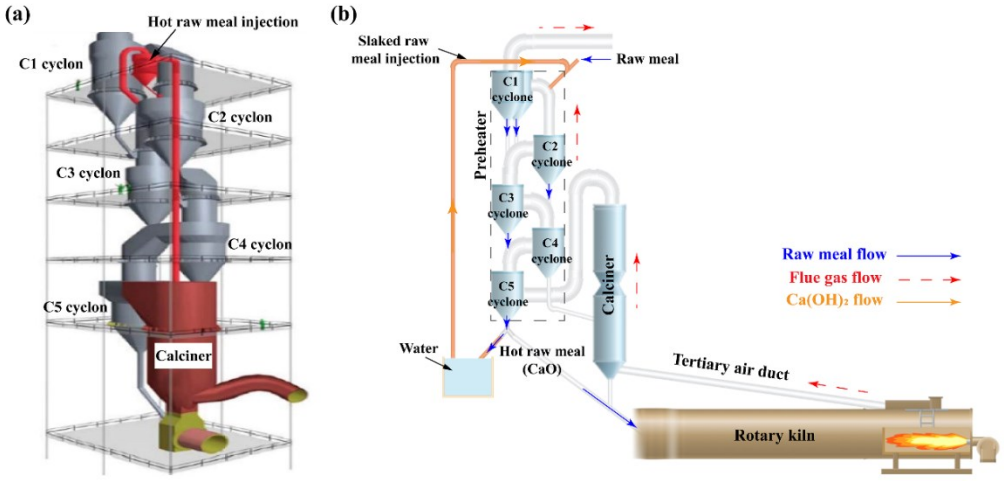

Fig. 3. Schematic diagrams of process compatible dry FGD technologies in cement industry: (a) Hot raw meal injection; (b) Slaked raw meal injection.

Since the above dry FGD technologies present low de-SO_2 efficiency, they cannot meet the increasingly higher requirement of SO_2 emission. The process compatible FGD technology is regarded as the development trend of the cement industry in the future, as de-SO_2 can be achieved using calcium-based adsorbents produced in the NSP cement production process. Given that the reactions between SO_2 and calcium-based

sorbents are typically slow and reversible gas-solid reactions (Li et al., 2012; Tullin and Ljungstroem, 1989) (**Fig. 4a**), it can be deduced that the de-SO_2 efficiency of current traditional FGD technologies are much less than expected. Therefore, the key to improving the efficiency of process compatible FGD technology is to accelerate chemical reactions during SO_2 capture.

Theoretically, SO_3 is much more reactive than SO_2, and the reactions between SO_3 and calcium-based adsorbents are no longer reversible (He et al., 2019; Wang et al., 2018). The product ($CaSO_4$) is much more stable than $CaSO_3$ (Ingo et al., 2001; Ma et al., 2022). Furthermore, SO_3 can react with moisture in the flue gas to form H_2SO_4, and then be rapidly captured by massive $CaCO_3$ in raw meal. Therefore, once SO_2 is oxidized to SO_3, the consequent capture will be much easier and more efficient even by the same calcium-based adsorbents (**Fig. 4b**). By introducing mineralizer, higher proportion of $CaSO_4$ reacts with CaO and Al_2O_3 to form calcium sulphoaluminate (Idrissi et al., 2010; Simoni et al., 2021), which has superior thermal stability than other sulfur-containing minerals during clinkerization (Cheng et al., 2003). Thus, more sulfur can be solidified in clinker and then discharged out of the kiln system, and less sulfur is involved in the kiln-preheater cycle, thereby reducing the amount of SO_2 that needs to be captured.

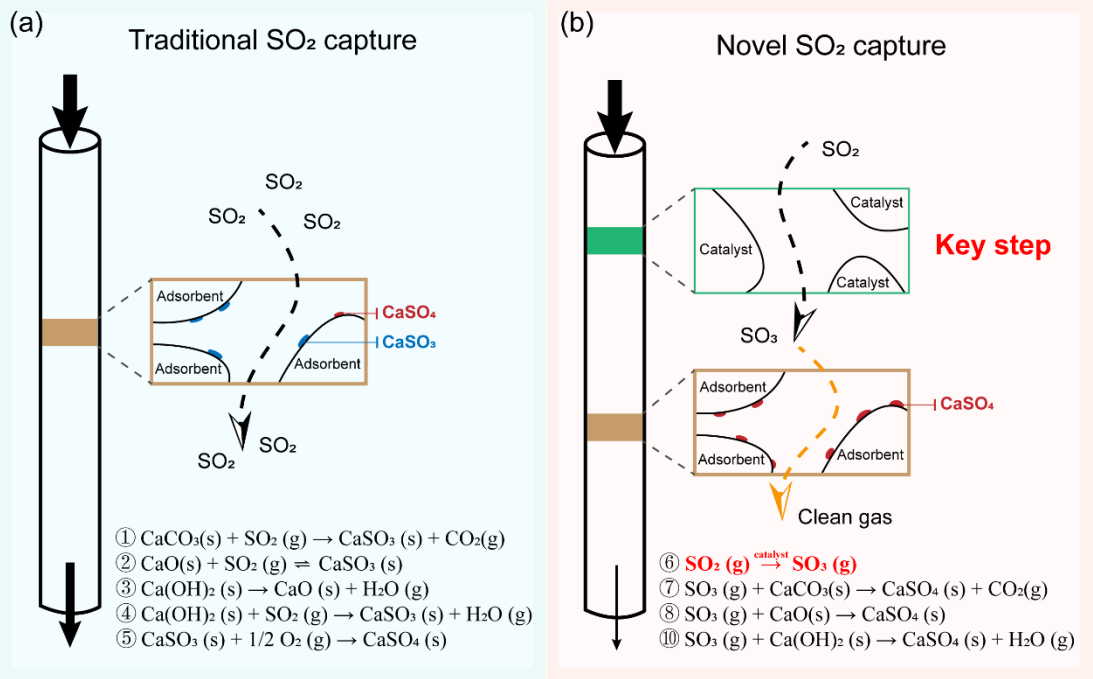

Fig. 4. Chemical reactions during SO_2 capture. (a) Traditional SO_2 capture by dry calcium-based adsorbents; (b) Novel SO_2 capture by combination of catalysts and calcium-based adsorbents.

Based on the above novel strategy for SO_2 capture, oxidation of trace SO_2 in the preheater environment has been achieved in our previous study by introducing V_2O_5-based catalysts, thus rapid capture gaseous SO_3 using calcium-based adsorbents (massive $CaCO_3$ in raw meal is preferred) is the critical step to develop high efficiency process compatible FGD technology. The velocity of flue gas in preheater is as high as 8-10 m/s, the contact time between gas and raw meal is only 3-5 s, and a high concentration of CO_2 (about 30-35%) in the flue gas can also react with adsorbents competitively, all of which increase the difficulty of gaseous SO_3/SO_2 capture. Up to now, the feasibility of rapid capture of trace SO_3/SO_2 in the preheater environment has not been evaluated yet.

In the present study, $CaCO_3$, CaO, and $Ca(OH)_2$ were selected to verify their potential for rapid capture of SO_2 in the preheater environment, and the effects of V_2O_5-based catalysts on the de-SO_2 efficiency and the corresponding mechanism were further studied. Subsequently, a novel process compatible FGD technology was designed for NSP cement production process, and industrial-scale trial was conducted to validate its feasibility and impacts on clinker properties. The results were of great significance to maximize the de-SO_2 potential of NSP cement production process and then improve the efficiency of available calcium-based dry FGD technology for the cement industry.

2 SO_2 capture efficiency of calcium-based adsorbents in simulated preheater environment

A fixed-bed reaction system, as shown in **Fig. 5**, was established to evaluate the SO_2 capture performance of $CaCO_3$, CaO, and $Ca(OH)_2$ in a simulated preheater environment (**Table 3**), and SiO_2 powder (inert material) was used as a reference. Pure O_2, SO_2, N_2, CO_2, and H_2O (introduced by a separate N_2 source through a thermostatic water bath) were mixed homogeneously in the gas mixer, and then simulated flue gas with target composition was obtained by controlling the flow rate of each gas component using separate mass flowmeters. It should be noted that a much higher SO_2 concentration (1.0 Vol.%) was selected to amplify the differences in SO_2 capture ability of the calcium-based absorbents, then de-SO_2 products in absorbents can be identified to clarify the SO_2 capture mechanism. Subsequently, the simulated flue gas was inlet into the temperature-controlled fixed-bed reactor, where 2.0 g catalyst (if required) and

20 g absorbent with the BET surface area of 320 ± 20 m^2/kg were dispersed separately in multilayer asbestos and then fixed in the quartz tube with size of φ 16 mm, as shown in **Fig. 5b**. The simulated flue gas permeated through the catalyst and absorbent layers in sequence at a flow rate of 1.0 L/min, in this case the time of flue gas passing through the absorbent layer was 4.0 s, which was equal to the actual contact time of gas-solid in the C1 and C2 cyclones of the industrial NSP process. Since part of SO_2 in the inlet flue gas was finally captured in the form of sulfate or sulfite, the SO_3 content of calcium-based absorbents after reaction for 5 min was tested to evaluate their SO_2 capture ability. Specifically, 1.0 g of the reacted absorbent was added into 20 ml $BaCl_2$-HNO_3 solution (100 g/L $BaCl_2$ and 4.0 mol/L HNO_3) with stirring for 30 min, and then the solution was rested for 24 h to ensure a full reaction. Finally, the precipitate ($BaSO_4$) in the solution was filtered and weighed after burning to constant weight at 850 ± 20 ºC, and then the SO_3 content of reacted absorbent was calculated according to **Eq. 1**.

$$\omega_{SO_3} = \frac{m_{BS} \times 0.343}{m_{ab}} \times 100\% \quad (1)$$

Where, ω_{SO_3} is the SO_3 content of reacted absorbent, %; m_{BS} is the mass of $BaSO_4$, g; m_{ab} is the mass of reacted absorbent, 1.0 g in this experiment; 0.343 is the mass ratio of SO_3 to $BaSO_4$.

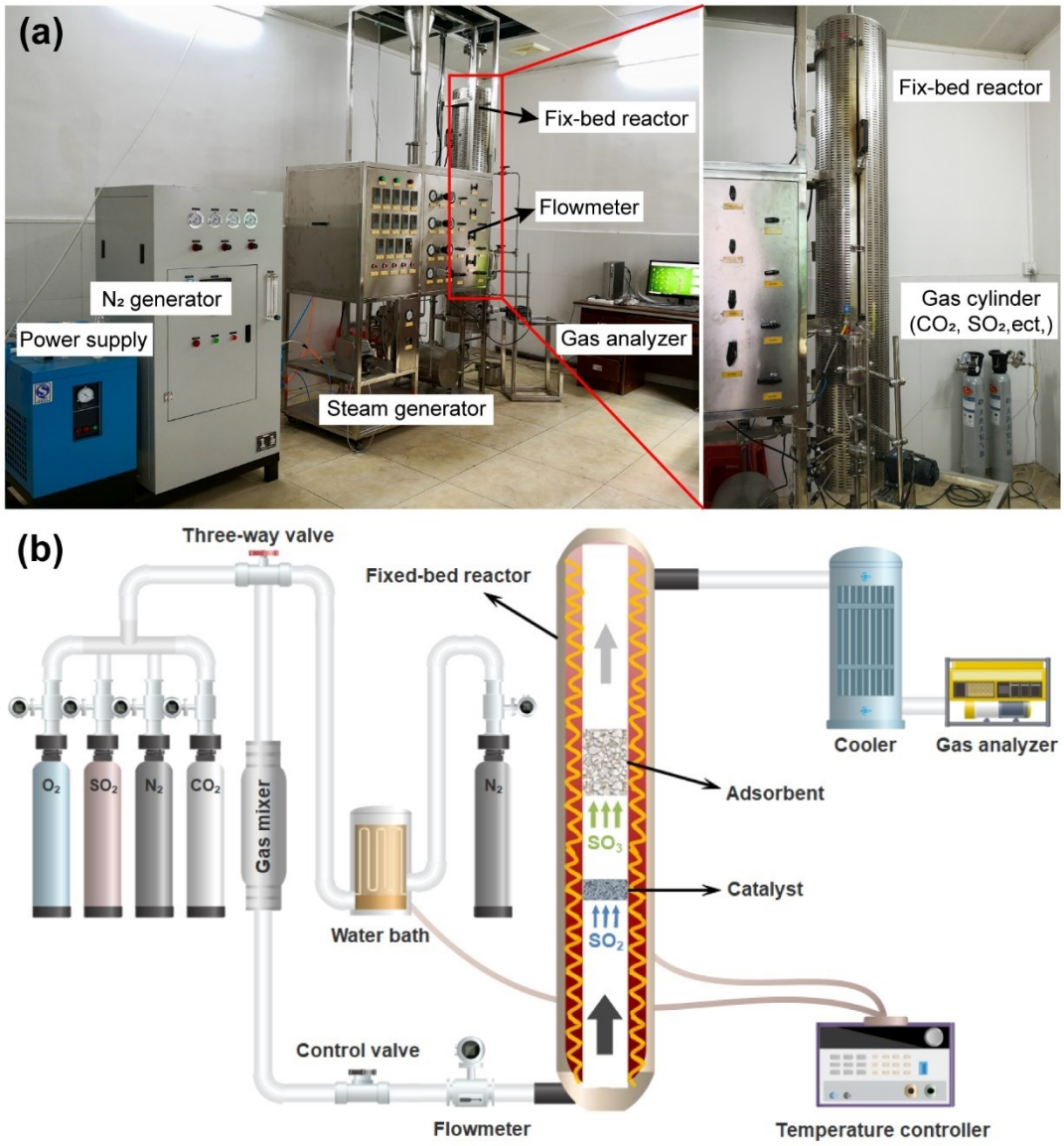

Fig. 5. Fixed-bed reaction system to evaluate the SO_2 capture performance of calcium-based absorbents in simulated preheater environment: (a) Equipment photograph; (b) Schematic diagram.

Table 3

Calcium-based adsorbents and environmental parameters of SO_2 capture test.

Adsorbent	Flue gas composition	Reaction conditions

SiO_2 $CaCO_3$ CaO $Ca(OH)_2$	1.0% SO_2 + 4.0% O_2 + 25.0% CO_2 + N_2 (Balance)	Gas flow: 1.0 L/min Volumetric space velocity: 2000/h Temperature: 600±10 ºC

209

210 2.1 SO_2 capture performance of $CaCO_3$, CaO, and $Ca(OH)_2$

211 As shown in **Fig. 6a**, SiO_2 powder had no SO_2 capture ability, as the SO_3 content
212 was only 0.02% after the reaction. Similarly, the SO_3 content when $CaCO_3$ powder was
213 used after reaction was as low as 0.07%, suggesting that $CaCO_3$ had nearly no SO_2
214 capture capability in a simulated preheater environment. That's why raw meal presented
215 neglectable SO_2 capture ability, when the flue gas passed through the whole preheater.
216 However, both CaO and $Ca(OH)_2$ powders showed relatively better SO_2 capture ability,
217 as the SO_3 contents of CaO and $Ca(OH)_2$ after reaction were 2.01% and 12.35%,
218 respectively. Thus, external $Ca(OH)_2$ or CaO was added with raw meal to capture SO_2
219 in the preheater in present dry FGD technologies, and $Ca(OH)_2$ generally had superior
220 SO_2 capture efficiency than CaO.

221 To identify the de-SO_2 products, X-ray diffraction (XRD) analysis of reacted
222 absorbents was carried out on a Bruker D8 advanced instrument operating at 250 mA
223 and 40 kV using Cu Kα1 radiation (λ = 0.1789 nm), and all tests were performed from
224 5º to 90º (2θ) with a step size of 0.02° and a scan speed of 8º/min. It can be seen from
225 **Fig. 6b** that no sulfur-containing mineral was identified in $CaCO_3$ and SiO_2 powders

after reaction, while $CaSO_3$ and a small amount of $CaSO_4$ were found in the XRD pattern of CaO powder after reaction. It can be concluded that SO_2 can be captured by CaO in the form of sulfite, which partially be oxidized to sulfate. Furthermore, the diffraction peaks of $CaSO_3$ were more pronounced in the XRD pattern of $Ca(OH)_2$ powder after the reaction, indicating more SO_2 was captured due to the high reactivity of $Ca(OH)_2$. It should be noted that diffraction peaks assigned to CaO were also identified, suggesting that a certain amount of $Ca(OH)_2$ was decomposed to CaO in the simulated preheater environment, thereby reducing the efficiency of SO_2 capture due to the relatively low reactivity of CaO. Moreover, $CaSO_4$ was also detected due to the oxidization of $CaSO_3$ particularly in reacted $Ca(OH)_2$ powder. Since most $CaSO_3$ decomposed and released SO_2 again when falling down to bottom cyclones (> 650 ºC) with raw meal, the SO_2 can only be effectively captured in the preheater in the form of $CaSO_4$ after oxidation.

The morphological changes and element compositions of absorbents before and after reaction were characterized by a scanning electron microscope (SEM, Nano 430) under secondary electron (SE) imaging mode with an accelerating voltage of 10 kV and energy dispersive spectrum (EDS) mode with accelerating voltage of 20 kV, respectively. As shown in **Fig. 6c and d**, no morphological difference was found for SiO_2 particles, and even very fine particles on the surface of large-sized grain had no S element (only Si and O with a molar ratio of 2 was detected) after the reaction. **Fig. 6e** presented the typical cubic grains with a smooth surface before the reaction, and the

surface was covered with numerous nanoscale protrusions after the reaction (**Fig. 6f**). According to literatures (Bigham et al., 2005; Hu et al., 2007), the protrusion was regarded as $CaSO_3$ crystal generated by the reaction of $CaCO_3$ and SO_2, although S element wasn't identified after reaction due to its very low content. It can be deduced that SO_2 was captured by $CaCO_3$ in a simulated preheater environment but with a very slow reaction rate, resulting in extremely small $CaSO_3$ protrusions in such a short reaction time. No obvious morphological change was observed for CaO particles before and after SO_2 capture, but the S element contents of interest points after reaction were in the range of 0.95-4.49%, indicating SO_2 was indeed captured by CaO. In contrast, a much loose surface of $Ca(OH)_2$ particles was observed after SO_2 capture and the S element content of the dense zone (de- SO_2 product layer) was as high as 16.49%, which was significantly higher than that of the loose zone (the decomposed $Ca(OH)_2$, 4.86%). It means that SO_2 is primarily captured by $Ca(OH)_2$, rather than reacting with the CaO generated from $Ca(OH)_2$ decomposition However, the SO_2 capture efficiency of $Ca(OH)_2$ was still not satisfied in the actual application (such as $Ca(OH)_2$ dry FGD method), due to the slow reaction rate and very short contract time.

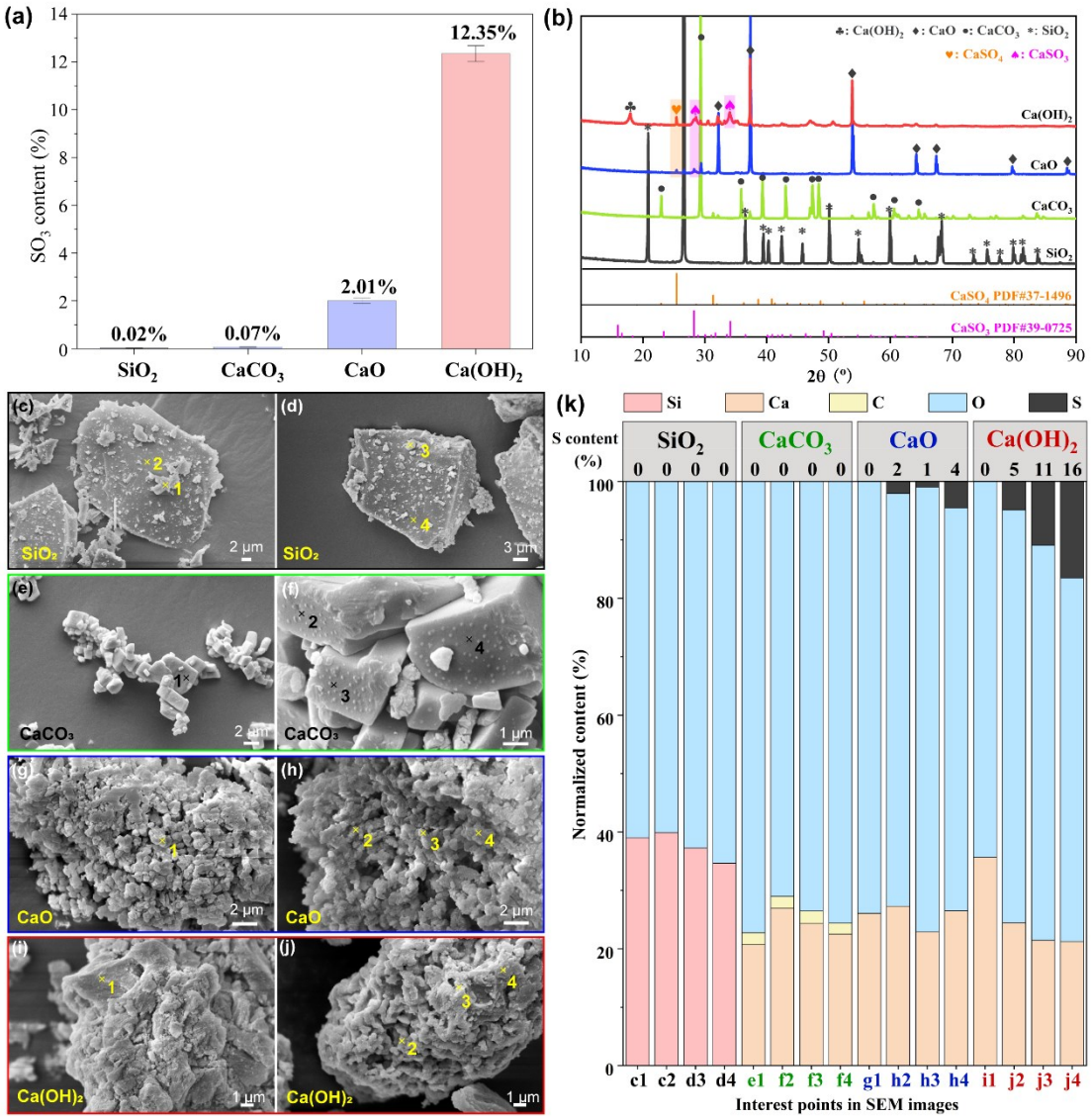

Fig. 6. SO_2 capture performance of calcium-based adsorbents: (a) SO_3 content of reacted adsorbents; (b) XRD patterns of reacted adsorbents; (c, d) SEM images of SiO_2 before and after reaction; (e, f) SEM images of $CaCO_3$ before and after reaction; (g, h) SEM images of CaO before and after reaction; (i, j) SEM images of $Ca(OH)_2$ before and after reaction; (k) EDS elemental compositions of interest points in SEM images.

Since the homogeneous direct oxidation of SO_2 needs to cross an energy barrier of

161.9 kJ/mol (**Eq. 2**) (Cullis and Mulcahy, 1972; Jørgensen et al., 2007), almost no SO_2 can be oxidized to SO_3 in an industrial furnace environment. The mechanism of SO_2 capture by calcium-based adsorbents can be classified into SO_2 adsorption, chemical reaction, vacancy diffusion and grain growth (Cheng et al., 2003; Hu et al., 2008; Hu et al., 2006; Jeong et al., 2015; Qiu and Lindqvist, 2000), in which the adsorption of SO_2 is the rate-determining step as shown in **Fig. 7**. The adsorption behavior of SO_2 on $CaCO_3$, CaO, and $Ca(OH)_2$ surface presented wide difference, which can be attributed to their adsorption site density and diffusion rate of vacancy (He et al., 2022; Hu et al., 2006; Malaga-Starzec et al., 2004). Specifically, SO_2(s) is firstly adsorbed on the surface active sites of adsorbents to form SO_2(ad) via chemisorption (**Eq. 3**), and $CaCO_3$ grain has a small amount of surface CO_3^{2-} vacancies, which can adsorb SO_2 (**Fig. 7b**) with an adsorption activation energy of 523.2 kJ/mol (Zhang et al., 2022). In contrast, a larger amount of surface O sites of CaO grain can adsorb SO_2 (**Fig. 7c),** and the adsorption activation energy reduces to 141.5 kJ/mol (Sasmaz and Wilcox, 2008). Furthermore, SO_2 is easily adsorbed by abundant surface OH sites of $Ca(OH)_2$ grain (**Fig. 7d**), as the adsorption activation energy of SO_2 further reduces to only 52.9 kJ/mol (He et al., 2022).

$$SO_2\ (ad) + O_2(g) \rightarrow SO_3\ (ad) + 161.9\ kJ/mol \quad (2)$$

For the reaction step, SO_2(ad) reacts with CO_3^{2-}(s) of $CaCO_3$ grain to form SO_3^{2-}(s) with the regeneration of vacancy and CO_2 release (**Eq. 4**). Similarly, SO_2(ad) also reacts with O^{2-}(s) of CaO grain or OH^-(s) of Ca(OH) grain to form SO_3^{2-}(s) with the

regeneration of vacancy (**Eq. 5 and 6**). The presence of vacancies in ionic crystalline grain is known to be one of the basic preconditions for gas-solid reaction (Hu et al., 2007) , thus the density and diffusion rate of vacancies in absorbents also affect the SO_2 capture efficiency. $CaCO_3$ grain with high crystallinity has a large anion radius and strong ion binding, which reduces the density and diffusion rate of vacancies. However, it is easier to form vacancies in the CaO and $Ca(OH)_2$ grains, resulting in a relatively faster diffusion rate of vacancies due to their loose microstructure. As a result, $CaCO_3$ presents neglectable SO_2 capture ability in consideration of short contact time and trace SO_2 concentration. CaO and $Ca(OH)_2$ also show low SO_2 capture ability and efficiency, as the reaction of SO_3^{2-}(s) with Ca^{2+}(s) to form $CaSO_3$(s) is a typical reversible reaction **(Eq. 7)**. Although a small amount of $CaSO_3$ is oxidized to $CaSO_4$ **(Eq. 8),** $CaSO_3$ on the surface of the calcium-based absorbents is the main de-SO_2 product of the direct SO_2 capture process.

Direct SO_2 capture:

$$SO_2\ (g) + [\ ]_v\ (s) \rightarrow [SO_2]_v\ (ad) \quad (3)$$

$$CO_3^{2-}\ (s) + [SO_2]_v\ (ad) \rightarrow SO_3^{2-}\ (s) + CO_2\ (g) + [\ ]_v\ (s) \quad (4)$$

$$O^{2-}\ (s) + [SO_2]_v\ (ad) \rightarrow SO_3^{2-}\ (s) + [\ ]_v\ (s) \quad (5)$$

$$2OH^-\ (s) + [SO_2]_v\ (ad) \rightarrow SO_3^{2-}\ (s) + H_2O\ (g) + [\ ]_v\ (s) \quad (6)$$

$$Ca^{2+}\ (s) + SO_3^{2-}\ (s) \rightleftharpoons CaSO_3\ (s) \quad (7)$$

$$CaSO_3\ (s) + 1/2\ O_2\ (g/ad) \rightarrow CaSO_4\ (s) \quad (8)$$

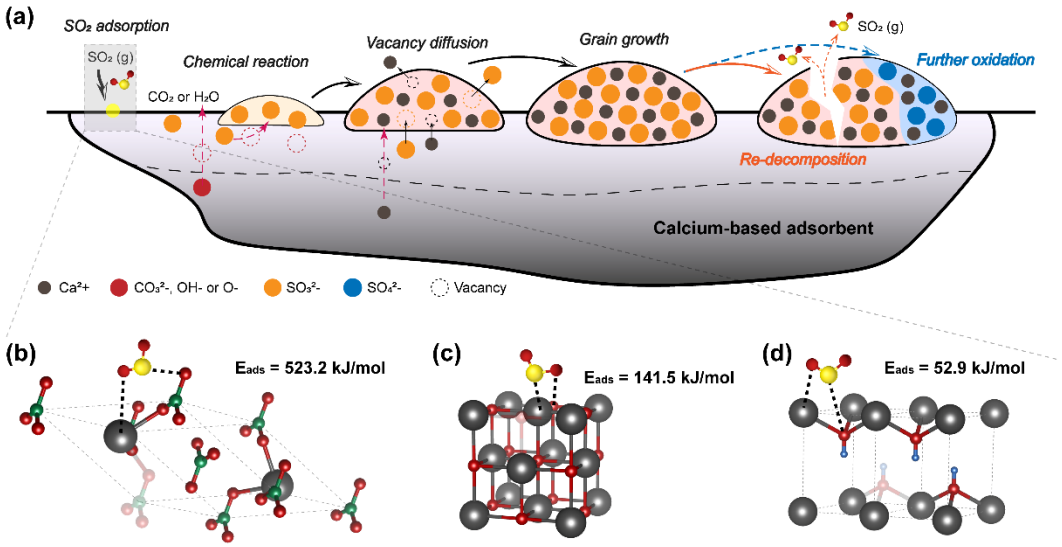

Fig. 7. Schematic illustration of SO_2 capture by calcium-based absorbents: (a) SO_2 capture process on the surface of calcium-based absorbent; (b) SO_2 adsorption on the active sites (CO_3^{2-} vacancy) of $CaCO_3$ grain; (c) SO_2 adsorption on the surface O sites of CaO grain; (d) SO_2 adsorption on the surface OH sites of $Ca(OH)_2$ grain.

2.2 Effect of V_2O_5-based catalysts and temperature on SO_2 capture capability

To improve the efficiency of SO_2 capture, V_2O_5-based catalysts were employed to catalyze the oxidation of SO_2 to SO_3, and the kinetics and mechanism of this reaction have been fully explored in our previous study (Wu, 2020). However, whether the synergism of V_2O_5-based catalysts and calcium-based adsorbents can improve the capture of SO_2 in the preheater remains to be investigated. Therefore, V_2O_5, V_2O_5-TiO_2, V_2O_5-MnO_2 and V_2O_5-CeO_2 (BET specific surface area of 173 ± 4 m^2/g, pore volume of 0.41 ± 0.03 cm^3/g, and an average pore diameter of 8.34 ± 0.09 nm.) were selected

as catalysts due to their excellent performance for catalytic oxidation of SO_2, and the simulated flue gas of typical preheater environment with normal moisture and SO_2 concentrations was used as shown in **Table 4**. The SO_2 in simulated flue gas contacted with catalysts and then reacted with adsorbents within 4.0 s, and the reaction temperatures were selected as 300 ºC, 400 ºC, 500 ºC, and 600 ºC (corresponding to outlet gas temperatures of C1, C2, C3, and C4 cyclones respectively). The SO_2 concentration of outlet flue gas was measured by a gas analyzer, and then SO_2 capture efficiency (φSO_2) was calculated by **Eq. 9**, which can provide a guideline for selecting the optimal location of catalyst-assisted de-SO_2 in NSP cement production process.

$$\varphi SO_2 = \frac{[SO_2]_{in} - [SO_2]_{out}}{[SO_2]_{in}} \times 100\% \quad (9)$$

where, $[SO_2]_{in}$ and $[SO_2]_{out}$ are the SO_2 concentrations of the inlet and outlet flue gas, respectively.

Table 4

Calcium-based adsorbents and environmental parameters of catalyst-assisted SO_2 capture test.

Absorbent	Catalyst	Flue gas composition	Reaction conditions
$CaCO_3$ CaO $Ca(OH)_2$	V_2O_5 V_2O_5-TiO_2 V_2O_5-MnO_2 V_2O_5-CeO_2	1000 ppm SO_2 + 4.0% O_2 + 25.0% CO_2 + 10.0% H_2O + N_2 (Balance)	Gas flow: 1.0 L/min Volumetric space velocity: 2000/h Temperature: 300, 400,500 and 600 ºC

As shown in **Fig. 8a,** the SO_2 capture efficiency of $CaCO_3$ powder increased from 0% up to 1.6% when the temperature increased from 300 ºC to 600 ºC. After adding

348 V_2O_5-based catalysts, nearly no change in the SO_2 capture efficiency was observed at
349 low temperatures (<400 °C). However, the SO_2 capture efficiency increased
350 significantly when the temperature surpassed 500 °C. For instance, the SO_2 capture
351 efficiency of $CaCO_3$ powder with V_2O_5-CeO_2 at 600 °C was 65.6%, which was 41 times
352 higher than that of pure $CaCO_3$. More importantly, $CaSO_4$ was detected as the main de-
353 SO_2 product rather than $CaSO_3$, indicating that SO_2 was firstly catalytic oxidized by
354 V_2O_5-CeO_2 and then captured by $CaCO_3$. For the same catalyst, CaO and $Ca(OH)_2$
355 powders presented slightly higher SO_2 capture efficiency (**Fig. 8c and e**). For example,
356 the combination of $Ca(OH)_2$ and V_2O_5-CeO_2 achieved the maximum SO_2 capture
357 efficiency of 75.5% at 600 °C.

358 Notably, $CaSO_3$ was identified as the predominate de-SO_2 product in the XRD
359 patterns of CaO at 400 °C (**Fig. 8d**), and $CaSO_4$ became the predominate de-SO_2 product
360 at 500 °C and 600 °C. More obviously, $CaSO_3$ was identified as the only de-SO_2 product
361 in the XRD patterns of $Ca(OH)_2$ at 600 °C without catalyst (**Fig. 8f**), and the diffraction
362 peaks of $CaSO_3$ in $Ca(OH)_2$ powder reduced sharply with the increase of reaction
363 temperature, accompanying with more and more pronounced $CaSO_4$ diffraction peaks.
364 It can be inferred that a small amount of SO_2 was directly captured by calcium-based
365 adsorbents (particularly for $Ca(OH)_2$), as the SO_2 in the flue gas was not effectively
366 catalytic oxidized over V_2O_5-based catalysts at low temperatures. In contrast, when the
367 reaction temperature surpassed 400 °C, more SO_2 was catalytically oxidized to SO_3,
368 which was easily and rapidly captured in the form of $CaSO_4$ even by $CaCO_3$ powder.

Thus, the raw meal in the preheater can be potentially used as an absorbent to capture SO_2 in the presence of V_2O_5-based catalysts.

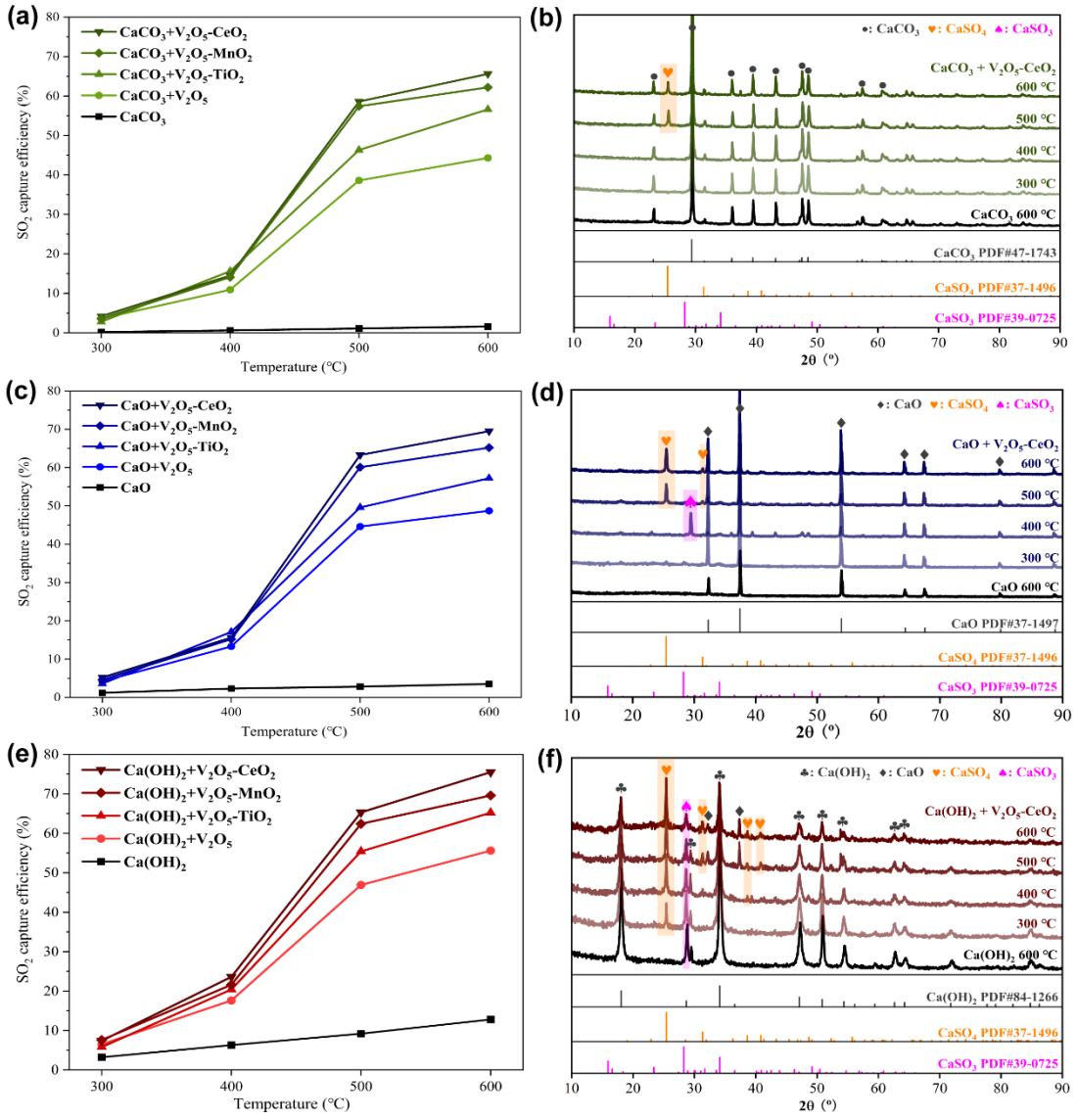

Fig. 8. Catalyst-assisted SO_2 capture performance: (a) & (b) SO_2 capture efficiency and XRD patterns of $CaCO_3$ powder; (c) & (d) SO_2 capture efficiency and XRD patterns of CaO powder; (e) & (f) SO_2 capture efficiency and XRD patterns of $Ca(OH)_2$ powder.

Based on the above experimental results, catalytic oxidation of SO_2 was the key

step to improving de-SO_2 efficiency. The mechanism of SO_2 capture by catalyst-assisted calcium-based absorbents was summarized in **Fig. 9**. Gaseous SO_2 and O_2 were adsorbed on the active sites (V=O or -O-V-O-) of the catalyst surface, and then most of the SO_2 was preferentially catalytically oxidized by neighboring O_2(ads) or O· to form SO_3 (**Eq. 10**) when passing through the V_2O_5-based catalysts layer. Meanwhile, part of SO_3 reacted with gaseous H_2O in the flue gas to form H_2SO_4 (Pei et al., 2023), which was rapidly captured by calcium-based absorbents (**Eq. 11-15**). The rest of SO_3 was also much easier captured (**Eq. 16-18)** compared to SO_2 (**Eq. 3-7**), as the reduction of SO_3 adsorption activation energy on the adsorbent surface (He et al., 2022; Liu et al., 2022).

Notably, the reaction between SO_3 and calcium-based absorbents was no longer reversible reactions (He et al., 2019; Kocaefe et al., 1985), and $CaSO_4$ had much higher thermal stability in the preheater environment than $CaSO_3$ (Wang et al., 2019; Zhang et al., 2013). All of these resulted in a much higher SO_2 capture efficiency. That is to say, by inducing V_2O_5-based catalysts and humidification, the de-SO_2 process was significantly accelerated by changing traditional slow reversible gas-solid reactions between SO_2 and calcium-based absorbents to much more rapid irreversible gas-solid reactions between H_2SO_4 droplets or even SO_3 and calcium-based absorbents, thereby resulting in a significant higher de-SO_2 efficiency even for $CaCO_3$ powders.

Catalyst-assisted SO_2 capture:

$$SO_2\,(ad) + O_2(g) \xrightarrow{Catalyst} SO_3\,(ad) \quad (10)$$

$SO_3\ (g) + H_2O\ (g) \rightarrow H_2SO_4\ (g)$ (11)

$H_2SO_4\ (g) \rightarrow H_2SO_4\ (ad)$ (12)

$H_2SO_4\ (ad) + CaCO_3\ (s) \rightarrow CaSO_4\ (s) + H_2O\ (g) + CO_2\ (g)$ (13)

$H_2SO_4\ (ad) + CaO\ (s) \rightarrow CaSO_4\ (s) + H_2O\ (g)$ (14)

$H_2SO_4\ (ad) + Ca(OH)_2\ (s) \rightarrow CaSO_4\ (s) + 2H_2O\ (g)$ (15)

$SO_3\ (ad) + CaCO_3\ (s) \rightarrow CaSO_4\ (s) + CO_2\ (g)$ (16)

$SO_3\ (ad) + CaO\ (s) \rightarrow CaSO_4\ (s)$ (17)

$SO_3\ (ad) + Ca(OH)_2\ (s) \rightarrow CaSO_4\ (s) + H_2O\ (g)$ (18)

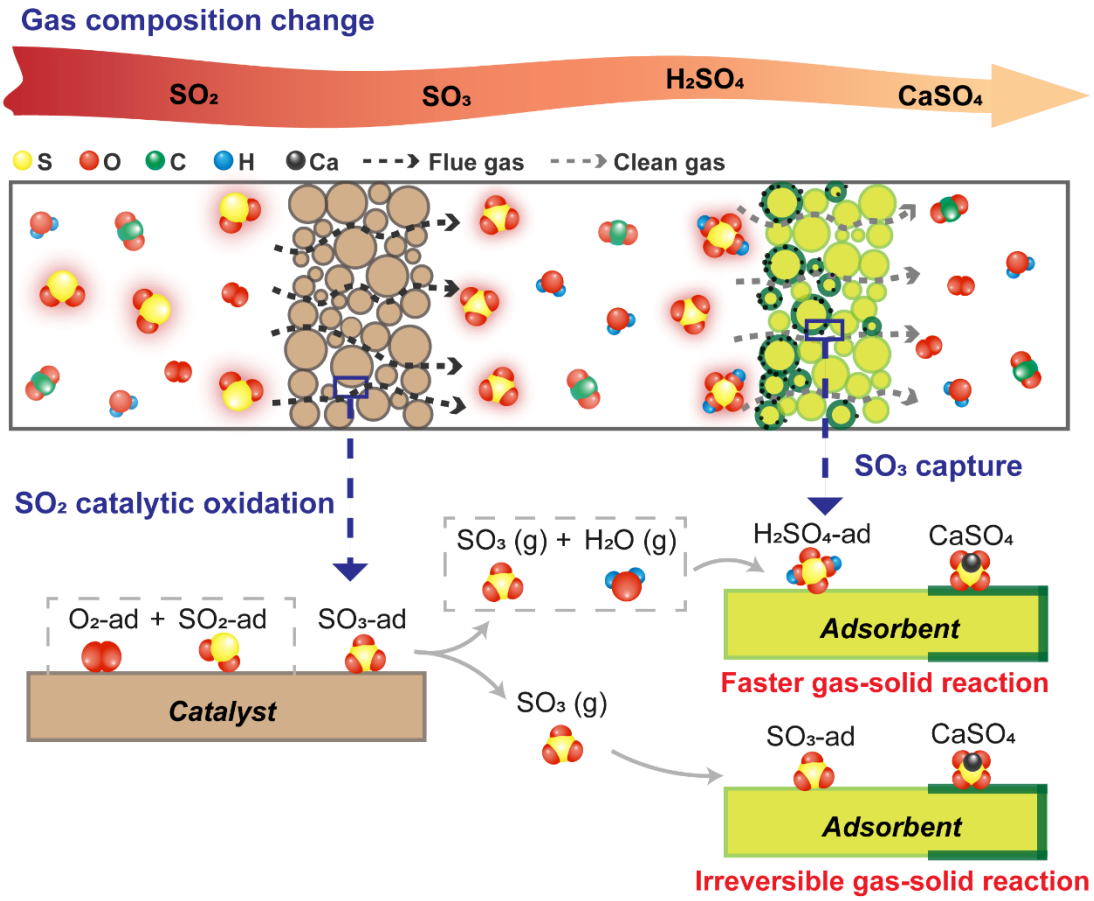

Fig. 9. Schematic illustration of catalyst-assisted SO_2 capture by calcium-based absorbents.

3 Design of process compatible FGD of NSP cement production

As mentioned above, catalytic oxidation and then efficient capture of SO_2 have been achieved in the simulated preheater environment, thus, how to realize these key steps on an industrial scale becomes the primary challenge of process compatible FGD, particularly in consideration of the characteristics of NSP production process. For solid flow, the raw meal moves downward from C1 cyclone to C5 cyclone after adding into the preheater, and the hot raw meal is clinkered in the rotary kiln after the decomposition of limestone in the pre-calciner. Meanwhile, flue gas moves upward (contrary direction with the solid flow) from cooler and rotary kiln to pre-calciner and then preheater. Since SO_2 released from fuel combustion and sulfates decomposition can effectively be captured by massive CaO in pre-calciner and C5 cyclone, technical route design focused on capturing SO_2 released by the oxidation of sulfide (mainly FeS_2, **Eq. 1 in Table 5**) in the preheater before flue gas discharge, specifically from C3 cyclone to C1 cyclone within only 3-5 s.

To achieve high de-SO_2 efficiency, the V_2O_5-based catalysts, calcium-based absorbent, and Ba-bearing mineralizer can be immediately suspended and completely dispersed by massive flue gas in C1 cyclone, after adding along with the raw meal as shown in **Fig. 10**. In this case, the catalysts can fully contact with flue gas in the whole process, and the SO_2 can be effectively oxidized to SO_3 immediately after being released in C3 cyclone or flowing up to C1 cyclone (**Eq. 2 in Table 5**). The newly formed SO_3 can react with massive fine limestone particles to form $CaSO_4$ directly in C3 and C2

cyclones (**Eq. 4 in Table 5**), and residual SO_3 is absorbed by liquid droplets to form H_2SO_4 when passing the duct accompanied with atomized humidifier between C2 and C1 cyclone (**Eq. 5 in Table 5**). Subsequently, the fine H_2SO_4 droplets are preferentially adsorbed on the surface of raw meal particles, and then react with limestone (liquid-solid reaction) to form $CaSO_4$ (**Eq. 6 in Table 5**), which is much more rapid and efficient compared with the original gas-solid reaction (Wang et al., 2015) (**Eq. 3 in Table 5**). Additionally, a small proportion of SO_2 and SO_3 escaped can be further captured by high active calcium-based absorbent (mainly $Ca(OH)_2$) (**Eq. 7 in Table 5**), so as to maximize the SO_2 capture capacity of the preheater section and then reduce the desulfurizer consumption and maintenance cost.

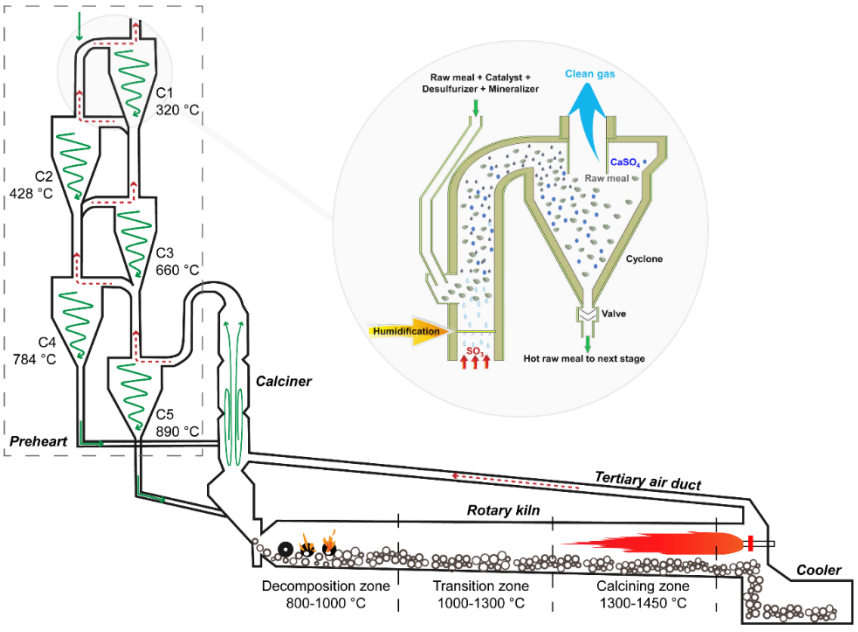

Fig. 10. Schematic diagram of compatible FGD design for NSP cement production process.

Generally, about 40-60% of $CaSO_4$, the FGD product, tends to decompose after entering the rotary kiln with hot raw meal (**Eq. 11 in Table 5**) (Li et al., 2014; Staněk,

2016), and the rest of $CaSO_4$, as well as alkali sulfates, are discharged out of the NSP production process with clinker. Theoretically, $CaSO_4$ can react directly with CaO and Al_2O_3 at 1250-1300 ºC to form $3CaO·3Al_2O_3·CaSO_4$ (**Eq. 12 in Table 5**), which presents better thermal stability and lower decomposition ratio during clinkerization (Wang et al., 2019). Furthermore, Ca^{2+} in $3CaO·3Al_2O_3·CaSO_4$ can be substituted by Ba^{2+}, and the generated Ba-bearing calcium sulphoaluminate (**Eq. 13 in Table 5**) had superior thermal stability (Cheng et al., 2000; Zhu et al., 2021). Ba-bearing wastes are also added with raw meals as mineralizer to stabilize the sulfur-containing minerals and reduce the sulfur cycling, a higher proportion of sulfur is therefore solidified in clinker and then discharged out of the rotary kiln rather than released as SO_2 in the flue gas.

457 Table 5

458 Chemical reactions occurred during NSP cement production before and after compatible FGD design.

459

Reaction site	Traditional NSP production		Illustration	Compatible FGD NSP production		Illustration
C3 cyclone (500-600 °C)	$2FeS_2 + 5.5O_2 \rightarrow Fe_2O_3 + 5SO_2$	(1)	SO_2 release	$2FeS_2 + 5.5O_2 \rightarrow Fe_2O_3 + 5SO_2$ $2SO_2 + O_2 \rightarrow 2SO_3$	(1) (2)	SO_2 release Catalytic oxidation
C3-C2 cyclone (350-500 °C)	$SO_2 + CaCO_3 \rightarrow CaSO_3 + CO_2$	(3)	Very slow and reversible SO_2 capture	$SO_3 + CaCO_3 \rightarrow CaSO_4 + CO_2$	(4)	Fast SO_3 capture
C1 cyclone (300-400 °C)	$SO_2 + CaCO_3 \rightarrow CaSO_3 + CO_2$	(3)		$SO_3 + H_2O \rightarrow H_2SO_4$ $H_2SO_4 + CaCO_3 \rightarrow CaSO_4 + CO_2 + H_2O$ $SO_3 + Ca(OH)_2 \rightarrow CaSO_4 + H_2O$	(5) (6) (7)	Faster liquid-solid reaction Efficient SO_3 capture
C5-precalciner (850-950 °C)	$SO_2 + CaO \rightleftharpoons CaSO_3$ $CaSO_3 + O_2 \rightarrow CaSO_4$	(8) (9)	Reversible Hard to react	$SO_3 + CaO \rightarrow CaSO_4$	(10)	More effective
Rotary kiln (1000-1450 °C)	$CaSO_4 \rightarrow CaO + SO_2 + O_2$ $CaSO_4 + CaO + Al_2O_3 \rightarrow 3CaO{\cdot}3Al_2O_3{\cdot}CaSO_4$	(11) (12)	Partially decomposed Solidification	$CaSO_4 \rightarrow CaO + SO_2 + O_2$ $CaSO_4 + CaO + Al_2O_3 \rightarrow 3CaO{\cdot}3Al_2O_3{\cdot}CaSO_4$ $CaSO_4 + BaO + CaO + Al_2O_3 \rightarrow (4\text{-}x)CaO{\cdot}xBaO{\cdot}3Al_2O_3{\cdot}SO_3$	(11) (12) (13)	Partially decomposed Solidification Solidification of Ba-bearing minerals

4 Industrial trial of process compatible FGD

4.1 Process and de-SO_2 efficiency

In order to evaluate the feasibility of process compatible FGD designed, an industrial trial was carried out on a 5000 t/d NSP production line in Huizhou, Guangdong province, China. Details of the NSP production process and environmental parameters of the connect duct between C2 cyclone and C1 cyclone for process compatible FGD are listed in **Table 6**. Since a small amount of FeS_2 was identified in the limestone used (**Fig. 11**), the SO_3 content of raw meal was as high as 0.9%, leading to a SO_2 emission of 800-1100 mg/Nm^3. According to the national emission standard , the upper limitation of SO_2 concentration in the flue gas of cement plants was 100 mg/Nm^3 for Guangdong province. Thus, low-cost and high-efficiency process compatible FGD is urgently needed to reduce SO_2 emissions. To reduce the cost of the industrial trial, tailings containing V_2O_5 and CeO_2 and industrial barium slag were used as catalysts and mineralizer, respectively, and commercial $Ca(OH)_2$ was selected as an external calcium-based absorbent. By changing the proportion of tailings, barium slag and $Ca(OH)_2$, target components of desulfurizer were controlled in the range of 4-5% V_2O_5, 2-3% CeO_2, 1-3% BaO, and 80-90% $Ca(OH)_2$. The chemical composition of a typical desulfurizer used in the industrial trial is listed in **Table 7**. To evaluate the effect of humidity of flue gas on the de-SO_2 efficiency, water was injected into the connect duct between C2 cyclone and C1 cyclone. Four double-fluid spray nozzles with 0.3 MPa high-pressure air were employed and uniformly arranged around the duct to ensure

481 homogeneous humidification (**Fig. 12**).

482 Table 6

483 Specification of the NSP production and environmental parameters of the connect duct

484 between C2 cyclone and C1 cyclone for process compatible FGD.

Parameter	Value	Units
Kiln type	Preheater-precalciner-rotary kiln	-
Preheater	5 cyclone stages	-
Clinker production capacity	5000	t/d
Control index		
KH	0.9±0.1	-
SM	2.2±0.1	-
IM	1.5±0.1	-
Raw materials	Limestone, clay, shale	-
Sulphur content of raw meal	0.898[a]	%
Fuel	Coal	-
Sulphur content of fuel	1.23[a]	%
Flue gas temperature and composition at connect duct between C2 and C1 cyclones		
Temperature	420±20	^{o}C
N_2	59.1±0.2	vol%
CO_2	32.0±1	vol%
CO	0.02±0.002	vol%
O_2	3.2±0.1	vol%
H_2O	5.5±0.3	vol%
SO_2	1500±100	mg/Nm^3
NO_x	390±50	mg/Nm^3
SO_2 concentration in exhaust flue gas	800-1100[b]	mg/Nm^3

485 Note: [a] In terms of SO_3; [b] After raw mill captures

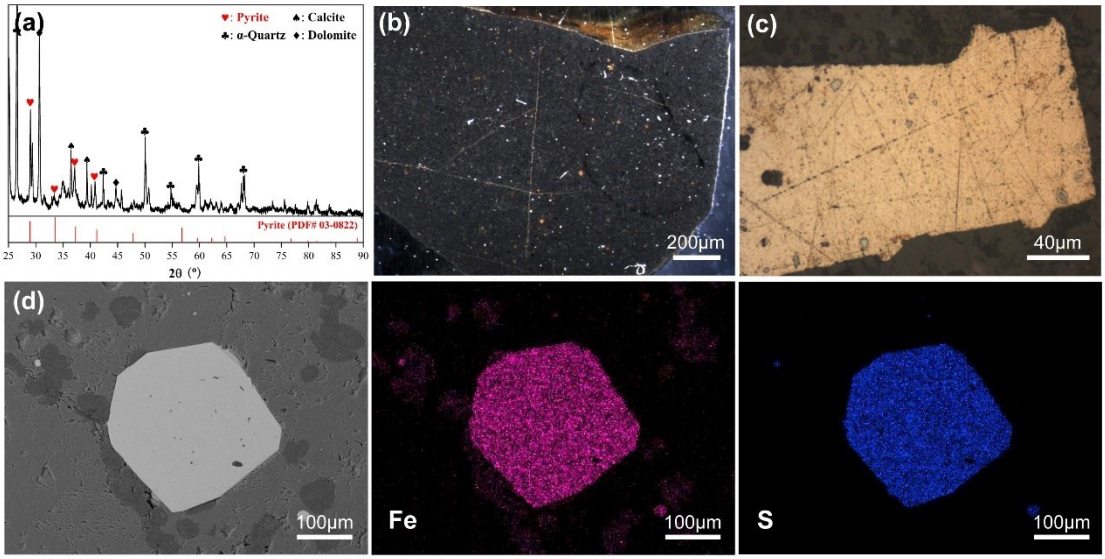

Fig. 11. Limestone collected from the 5000 t/d NSP production line. (a) XRD pattern; (b) Optical image; (c) Polarized light image of pyrite; (d) Back Scattered Electron image and distributions of Fe and S.

Table 7

Chemical composition of desulfurizer used in the industrial trial (wt.%).

V_2O_5	CeO_2	BaO	CaO	Al_2O_3	Fe_2O_3	SiO_2	LOI*	Others
4.68	2.31	1.93	64.10	2.37	1.48	1.18	19.13	2.82

Note: *, loss on ignition.

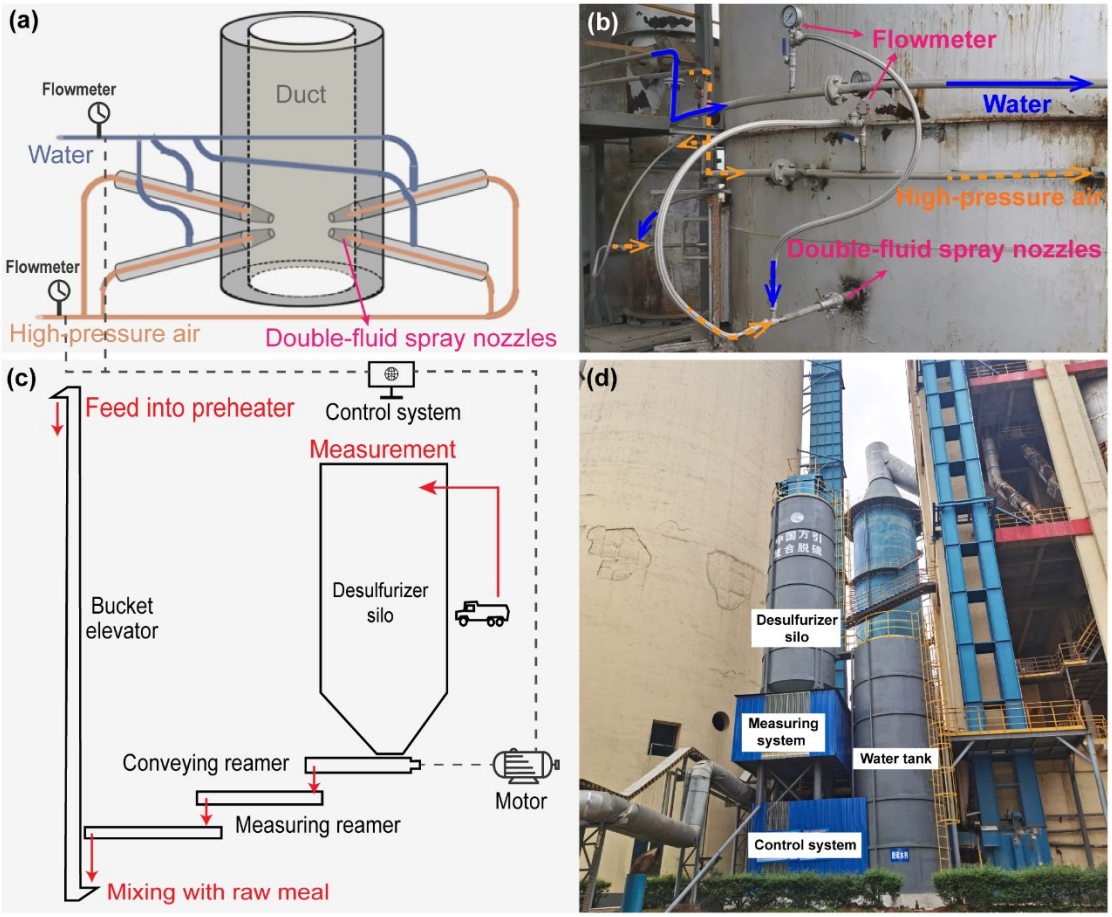

Fig. 12. Equipment for humidification and desulfurizer adding process. (a) Schematic diagram of double-fluid spray nozzles and their locations; (b) Photograph of the spray nozzles with the water and high-pressure air supplies; (c) Schematic diagram of powder desulfurizer adding process; (d) Overview of desulfurizer silo and water tank.

During the industrial trial, a target amount of desulfurizer was added with raw meal, and the SO_2 concentration in the exhaust flue gas was on-site measured in real time. As shown in **Fig. 13a**, the SO_2 emission was in the range of 800-1100 mg/Nm^3 before adding desulfurizer, and then decreased significantly with the increase of desulfurizer to raw meal mass ratio. When the addition of desulfurizer increased to 0.5%, the SO_2

emission reduced to 126 mg/Nm^3 and then stabilized for 2.0 h, which can meet the general requirement of SO_2 emission. Moreover, SO_2 emission increased rapidly to about 1000 mg/Nm^3 after discontinuing desulfurizer adding. In contrast, the SO_2 emission was only reduced to 400-500 mg/Nm^3 when the addition of external $Ca(OH)_2$ of traditional dry FGD increased 3.0% relative to raw meal for the same NSP kiln, indicating that the de-SO_2 efficiency can be effectively promoted by adding catalyst. To reduce FGD cost, the combination effect of desulfurizer and humidification on the de-SO_2 efficiency was further evaluated. As shown in **Fig. 13b**, the SO_2 emission can be reduced to about 600-700 mg/Nm^3 when only desulfurizer was added (the mass ratio of desulfurizer to raw meal was 0.2 %). The SO_2 emission can further be reduced to 50-100 mg/Nm^3 after introducing 0.5 t/h water to humidify the flue gas, suggesting that the humidification of flue gas can increase de-SO_2 efficiency with a lower amount of desulfurizer. This may be attributed to the formation of H_2SO_4, which can be captured by the calcium-based absorbent or even limestone more rapidly. However, only a slight decrease in SO_2 emissions was observed when the injected water increased up to 1.0 t/h, and the SO_2 emission quickly returned to its initial level once stopping powder desulfurizer. It can be deduced that the powder desulfurizer plays a crucial role in the de-SO_2 process, and humidification can only promote the de-SO_2 process in the presence of desulfurizer. Furthermore, the process compatible FGD presented well-adaptability to a large fluctuation of SO_2 emission, because even if the SO_2 emission increased to 1100-1350 mg/Nm^3 due to the utilization of higher sulfur-containing

limestone, the SO_2 emission was still reduced to <100 mg/Nm^3 by a combination of desulfurizer and humidification. Additionally, a visually clean exhaust gas after process compatible FGD was observed**,** while that after wet FGD (limestone-gypsum method) had a long white smog (**Fig. 13c**) due to the presence of gypsum droplets (Liu et al., 2013; Lv et al., 2011; Pan et al., 2017; Shi et al., 2017).

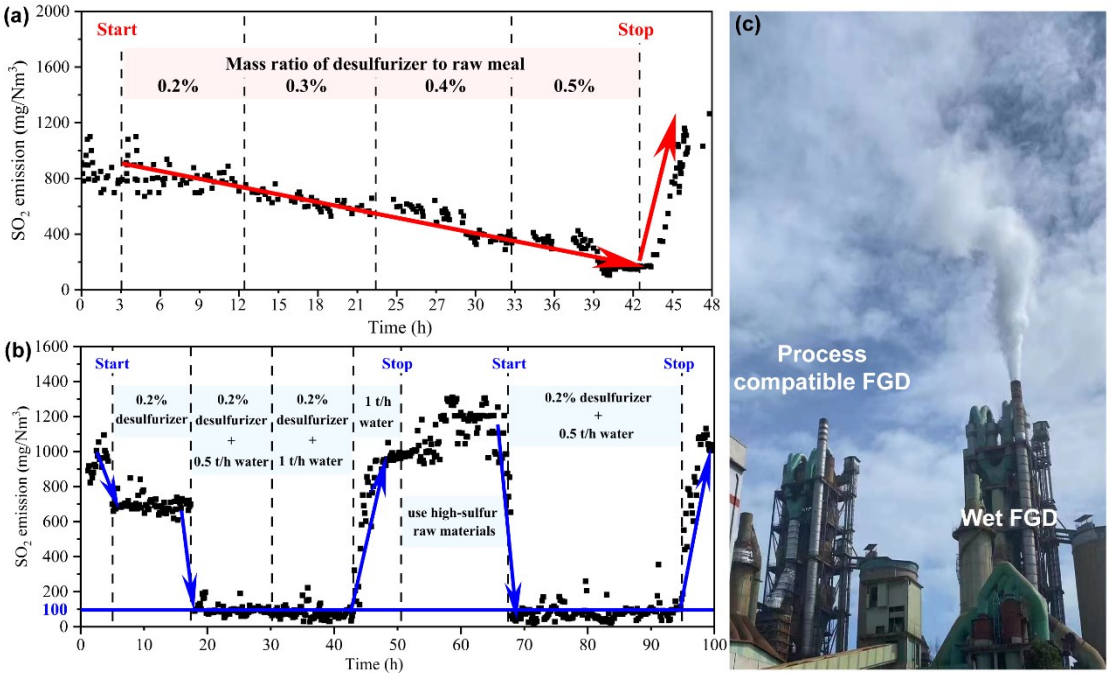

Fig. 13. SO_2 emission of the 5000 t/d NSP production line during industrial trial. (a) Influence of desulfurizer addition; (b) Influence of humidification; (c) Visual exhaust gas emission comparison of process compatible FGD and traditional wet FGD.

The properties of cement clinker before and after process compatible FGD were also compared to evaluate the influence of de-SO_2. XRF analysis showed that SO_3 content in the clinker after de-SO_2 reached 1.27%, which was higher than the initial value (0.98%). It can be seen from **Fig. 14a**, the S element was evenly dispersed in the

intermediate phase of the clinker before de-SO_2, while more S element was found in the form of alkali sulfates (mainly $3K_2SO_4 \cdot Na_2SO_4$), trace calcium sulphoaluminate and barium sulfoaluminate, which were enwrapped by intermediate phase after de-SO_2 (**Fig. 14b and c**). The XPS spectra (S $2p_{3/2}$) of the intermediate phase in the clinker also confirmed the presence of sulfates (Qiu et al., 2013) (**Fig. 14d**). After process compatible FGD, no obvious change in water requirement for normal consistency and setting times was observed for Portland cements with same specific surface area, but the 3-day and 28-day compressive strengths increased by 1.2 MPa and 1.5 MPa, respectively (**Table 8**). The phenomenon can be illustrated by the fact that calcium sulphoaluminate, one of desulfurization products, results in relatively higher early and later strengths due to rapid hydration and more ettringite generation (Bullerjahn et al., 2019; Gastaldi et al., 2016; Ma et al., 2021; Padilla-Encinas et al., 2021).

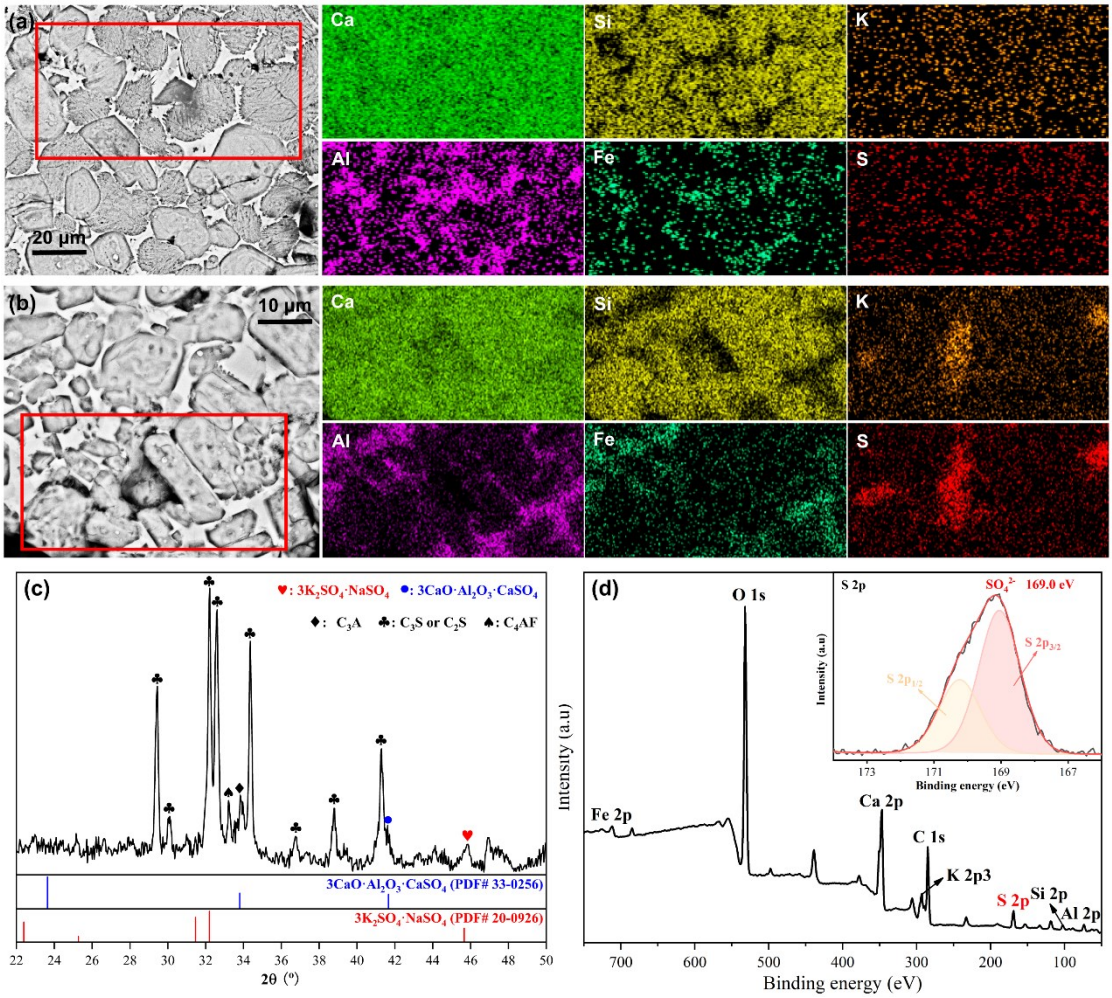

Fig. 14. Characterization of cement clinker before and after process compatible FGD. (a) Back Scattered Electron image and element distributions of clinker before FGD; (b) Back Scattered Electron image and element distributions of clinker after FGD; (c) XRD patterns of clinker after FGD; (D) XPS spectra (S $2p_{3/2}$) of the intermediate phase of clinker after FGD.

Table 8
Fundamental properties of Portland cement produced before and after process compatible FGD.

	Specific surface area (m^2/kg)	Water demand (%)	Setting time (min)		Compressive strength (MPa)		Flexural strength (MPa)	
			Initial	Final	3d	28d	3d	28d

Before	349	25.1	145	228	33.1±0.8	55.3±1.1	7.0±0.3	9.6±0.4
After	352	25.1	139	226	34.3±0.6	56.8±1.3	7.2±0.3	9.8±0.3

4.2 Sulfur balance calculation before and after process compatible FGD

The sulfur in the NSP cement production system was only introduced by raw meal and coal, then SO_2 in the flue gas was captured as solid sulfates by process compatible FGD. Part of the solid sulfates decomposed to release SO_2 when the temperature was higher than 1250 ºC, and the rest solid sulfates were discharged out with clinker. Meanwhile, most of SO_2 in the flue gas was then captured when pasting through pre-calciner, preheater, and raw mill, and trace SO_2 was emitted out with flue gas. That is to say, the input sulfur was only discharged out as solid sulfates in clinker or gaseous SO_2 in the flue gas. Theoretically, the amount of SO_3 introduced by raw meal and coal equaled to the total SO_3 amount in clinker and flue gas. In order to clarify the changes of sulfur pathway and validate the SO_2 capture efficiency, sulfur input and output of the NSP production system before and after process compatible FGD were calculated according to the SO_3 contents of limestone, raw meal, coal, and clinker (**Table 9**) and SO_2 concentration in the flue gas.

Table 9

The SO_3 contents and consumptions of raw meal, fuel, and clinker and SO_2 emission before and after process compatible FGD.

	Raw meal[a] (C_{rm}/ %)	Coal[a] (C_c/ %)	Clinker[a] (C_{cl}/ %)	SO_2 emission (E_g/ mg/Nm^3)
Before	0.90	1.23	1.34	1080±50

After	0.90	1.23	1.52	200±30
Consumption or discharging	380 t/h	33 t/h	245 t/h	400000 Nm^3/h

Note: [a] In terms of SO_3

Sulfur inputs

The amounts of SO_3 introduced by raw meal (m_{rm}) and coal (m_c) were calculated as follows:

$$m_{rm} = C_{rm} \times M_{rm} = 0.90\% \times 380\ t/h = 3.420\ t/h \quad (19)$$

$$m_c = C_c \times M_c = 1.23\% \times 33\ t/h = 0.406\ t/h \quad (20)$$

Sulfur outputs

The amounts of SO_3 discharged with clinker (Before: $m_{cl\text{-}b}$, After: $m_{cl\text{-}a}$) and exhaust gas (Before: $m_{g\text{-}b}$, After: $m_{g\text{-}a}$) were calculated:

Before:

$$m_{cl\text{-}b} = C_{cl\text{-}b} \times M_{cl} = 1.34\% \times 245\ t/h = 3.283\ t/h \quad (21)$$

$$m_{g\text{-}b} = E_{g\text{-}b} \times V_g \times m(SO_3)/m(SO_2) = 1080\ mg/Nm^3 \times 400000\ Nm^3/h \times 80/64 = 0.540\ t/h \quad (22)$$

After:

$$m_{cl\text{-}a} = C_{cl\text{-}a} \times M_{cl} = 1.52\% \times 245\ t/h = 3.724\ t/h \quad (23)$$

$$m_{g\text{-}a} = E_{g\text{-}a} \times V_g \times m(SO_3)/m(SO_2) = 200\ mg/Nm^3 \times 400000\ Nm^3/h \times 80/64 = 0.100\ t/h \quad (24)$$

As shown in **Fig.15**, the sulfur balance of the cement kiln system before and after process compatible FGD were established. Obviously, the sulfur input of the cement kiln system equaled to the sulfur output for the two situations, but more sulfur was solidified into clinker rather than SO_2 emission after process compatible FGD.

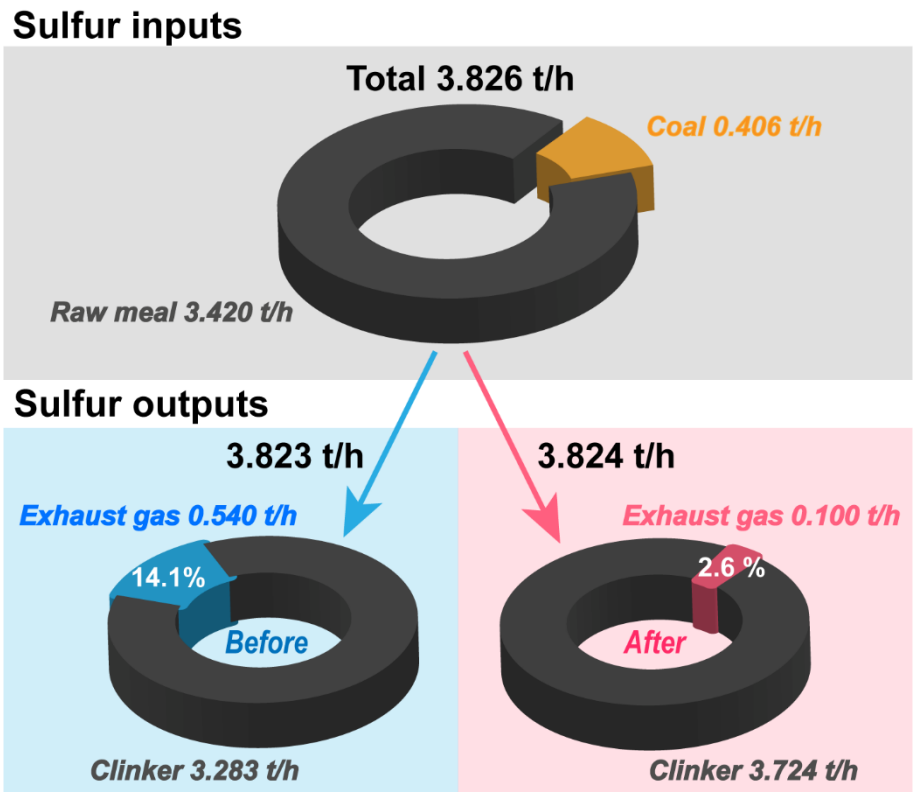

600

601 Fig. 15. Sulfur inputs and outputs of cement kiln system before and after process

602 compatible FGD.

603 4.3 Economic analysis and efficiency comparison

604 According to large-scale industrial trials and available literatures (Chang et al.,

605 2011; Duque et al., 2010; Yu et al., 2020), economic analysis and efficiency

606 comparisons among traditional dry FGD (hot raw meal or slaked raw meal injections),

607 wet limestone-gypsum FGD, and the process compatible FGD developed were listed in

608 **Table 10**. Traditional dry FGDs had simplified equipment, low investment and

609 maintaining cost by using CaO or $Ca(OH)_2$ from the cement kiln system, but generally

610 presented low de-SO_2 efficiency (30-50%) and then only applied to cement plants with

611 low SO_2 emission (<300 mg/Nm^3) Wet limestone-gypsum FGD was mainly applied in

612 cement plants with high SO_2 emission (> 1500 mg/Nm^3), as higher de-SO_2 efficiency

(> 95%) was achieved through multi-circulation of limestone slurry. However, complex equipment and high water and electricity consumptions were needed, leading to much higher investment and maintenance cost. In contrast, the equipment and investment of process compatible FGD were similar to those of traditional dry FGD, but the de-SO_2 efficiency was as high as that of wet FGD by introducing catalysts. Furthermore, the maintaining cost of process compatible FGD was about 5-20% of that of wet FGD or slight lower than that of traditional FGD, as most of SO_2 was captured by limestone in raw meal rather than external calcium-based absorbent, and most of catalysts components were introduced by solid wastes or tailings. Therefore, the process compatible FGD can be regarded as an efficient, low-cost, and adaptable technology for the cement industry, particularly for SO_2 emissions less than 2500 mg/Nm^3.

Table 10

Characteristics and efficiency comparison of traditional dry FGDs, wet FGD and process compatible dry FGD.

De-SO_2 technology	Hot raw meal (or external CaO) injection	Slaked raw meal (or external $Ca(OH)_2$) injection	Wet limestone-gypsum FGD	Process compatible dry FGD
Desulfurizer	CaO	$Ca(OH)_2$	Limestone slurry	Catalyst, $Ca(OH)_2$ and mineralizer
De-SO_2 efficiency	30-40%	50-60%	＞95%	＞95%
Influences on NSP process	Poor burnability	Increasing total heat consumption	Increasing gas flow resistance; De-SO_2 equipment pipe blockage	Reducing outlet gas temperature from C1 about 3-5 ^oC

Investment	About 1 million RMB	About 2 million RMB	About 15-20 million RMB	About 1 million RMB
Maintenance cost	Very low	Middle	High	Low
Main advantages	No absorbent consumption	Self-availability of absorbent	High adaptability and maturity	Low energy and water consumptions
Main disadvantages	Poor adaptability; Reducing clinker production capacity	Poor adaptability Complex system	Large and complex system; High water and electricity consumptions	Reducing heat recovery from waste gas
Economic SO_2 emission source	<200 mg/Nm^3	<300 mg/Nm^3	>1500 mg/Nm^3	<2500 mg/Nm^3

5 Conclusions and prospect

The following conclusions can be drawn from the present study:

1. $CaCO_3$ had nearly no SO_2 capture ability in the typical preheater environment, both $Ca(OH)_2$ and CaO presented a low de-SO_2 efficiency. Moreover, the main de-SO_2 product of calcium-based absorbents was $CaSO_3$ through reversible gas-solid reactions in such a short contact time and trace SO_2 concentration, and only a small amount of $CaSO_3$ was oxidized to $CaSO_4$ at preheater environment to finish SO_2 capture. After introducing V_2O_5-based catalysts, SO_2 was effectively oxidized to SO_3, which was more rapidly and efficiently captured by calcium-based absorbents to form $CaSO_4$ directly following irreversible gas-solid reactions. Finally, a maximum de-SO_2 efficiency of 75.5% was achieved at 600 °C using $Ca(OH)_2$ in the presence of V_2O_5-CeO_2 catalyst.

2. A novel process compatible FGD was proposed according to the characteristics of NSP cement klin system. The V_2O_5-based catalysts, calcium-based absorbent and Ba-bearing mineralizer were added with raw meal, and then completely suspended and dispersed by the massive flue gas from C1 cyclone to rotary kiln. As a result, the SO_2 released from decomposition of FeS_2 was effectively oxidized and then captured by massive limestone in the raw meal particularly when humidification at the duct between C2 and C1 cyclones. Finally, the de-SO_2 product ($CaSO_4$) took part in clinkerization to form sulfur-containing minerals with high thermal stability, then a larger amount of sulfur was discharged out with clinker.

3. In the industrial trial of process compatible FGD, the SO_2 concentration in the flue gas decreased rapidly from 1100-1350 mg/Nm^3 to <100 mg/Nm^3 after adding 0.2% desulfurizer (relative to raw meal) and 0.5 t/h H_2O, as more sulfur was solidified into clinker rather than emitted with flue gas as SO_2. Thus process compatible FGD can provide an efficient and economical approach to reducing SO_2 emission from the cement industry, and the results are of great significance in improving the efficiency of available calcium-based dry FGD technologies.

CRediT authorship contribution statement

Tongsheng Zhang: Conceptualization, Validation, Writing - original draft, review & editing, Supervision, Funding acquisition. **Hui Peng**: Data curation, Writing - original draft, Visualization, Investigation. **Chang Wu**: Validation, Data curation, Formal analysis. **Yiqun Guo & Jiawei Wang**: Validation, Modification, Visualization,

Writing - review. **Xinzhi Chen**: Investigation. **Jiangxiong Wei & Qijun Yu**: Supervision, Writing - review & editing.

Declaration of Competing Interest

The authors declare that they have no known competing financial interests or personal relationships that could have appeared to influence the work reported in this paper.

Acknowledgements

This work was funded by the National Natural Science Foundation of China (No. 51872096 & 52122201) and the Guangdong Science and Technology Program (2016A020221009 & 2021A0505030008). Their financial supports are gratefully acknowledged.

References

Emission standard of air pollutants for cement industry, Chinese standard GB 4915, 2013.

Bigham, J.M., Kost, D.A., Stehouwer, R.C., Beeghly, J.H., Fowler, R., Traina, S.J., Wolfe, W.E., Dick, W.A., 2005. Mineralogical and engineering characteristics of dry flue gas desulfurization products. Fuel 84(14-15), 1839-1848.

Borgwardt, R.H., 1970. Kinetics of the reaction of sulfur dioxide with calcined limestone. Environmental Science & Technology 4(1), 59-63.

Bueno-Lopez, A., Garcia-Garcia, A., 2005. Combined SO_2 and NO_x removal at moderate temperature by a dual bed of potassium-containing coal-pellets and calcium-containing pellets. Fuel Processing Technology 86(16), 1745-1759.

Bullerjahn, F., Boehm-Courjault, E., Zajac, M., Ben Haha, M., Scrivener, K., 2019. Hydration reactions and stages of clinker composed mainly of stoichiometric ye'elimite. Cement and Concrete Research 116, 120-133.

Bullerjahn, F., Schmitt, D., Ben Haha, M., 2014. Effect of raw mix design and of clinkering process on the formation and mineralogical composition of (ternesite) belite calcium sulphoaluminate ferrite clinker. Cement and Concrete Research 59, 87-95.

Chang, G.Q., Song, C.Y., Wang, L., 2011. A modeling and experimental study of

flue gas desulfurization in a dense phase tower. Journal of Hazardous Materials 189(1-2), 134-140.

Chen, R., Zhang, T.S., Guo, Y.Q., Wang, J.W., Wei, J.X., Yu, Q.J., 2021. Recent advances in simultaneous removal of SO_2 and NO_x from exhaust gases: Removal process, mechanism and kinetics. Chemical Engineering Journal 420.

Cheng, J., Zhou, J.H., Liu, J.Z., Zhou, Z.J., Huang, Z.Y., Cao, X.Y., Zhao, X., Cen, K.F., 2003. Sulfur removal at high temperature during coal combustion in furnaces: a review. Progress in Energy and Combustion Science 29(5), 381-405.

Cheng, X., Chang, J., Lu, L.C., Liu, F.T., Teng, B., 2000. Study of Ba-bearing calcium sulphoaluminate minerals and cement. Cement and Concrete Research 30(1), 77-81.

Cullis, C.F., Mulcahy, M.F.R., 1972. The kinetics of combustion of gaseous sulphur compounds. Combustion and Flame 18(2), 225-292.

Czyzewski, A., Kapica, J., Moszynski, D., Pietrzak, R., Przepiorski, J., 2013. On competitive uptake of SO_2 and CO_2 from air by porous containing CaO and MgO carbon. Chemical Engineering Journal 226, 348-356.

Duque, C., Montes, C., Bustamante, F., Ortiz, A., 2010. Simulation of two alternatives for SO_2 removal from wet cement kiln exhaust gases. Revista Facultad De Ingenieria-Universidad De Antioquia(56), 49-57.

Gao, T.M., Shen, L., Shen, M., Liu, L.T., Chen, F.N., 2016. Analysis of material flow and consumption in cement production process. Journal of Cleaner Production 112, 553-565.

Gastaldi, D., Paul, G., Marchese, L., Irico, S., Boccaleri, E., Mutke, S., Buzzi, L., Canonico, F., 2016. Hydration products in sulfoaluminate cements: Evaluation of amorphous phases by XRD/solid-state NMR. Cement and Concrete Research 90, 162-173.

Han, Y., Hwang, G., Kim, D., Park, S., Kim, H., 2015. Porous Ca-based bead sorbents for simultaneous removal of SO_2, fine particulate matters, and heavy metals from pilot plant sewage sludge incineration. Journal of Hazardous Materials 283, 44-52.

Hansen, J.P., Jensen, L.S., Wedel, S., Dam-Johansen, K., 2003. Decomposition and oxidation of pyrite in a fixed-bed reactor. Industrial & Engineering Chemistry Research 42(19), 4290-4295.

He, K., Tang, Z., Song, Q., Yao, Q., 2022. Process analysis of SO_3 removal by $Ca(OH)_2$ particles from flue gas. Chemical Engineering Science 247, 117054.

He, K.J., Song, Q., Yan, Z.N., Zheng, N., Yao, Q., 2019. Study on competitive absorption of SO_3 and SO_2 by calcium hydroxide. Fuel 242, 355-361.

Hu, G., Dam-Johansen, K., Wedel, S., 2008. Oriented nucleation and growth of anhydrite during direct sulfation of limestone. Crystal Growth & Design 8(4), 1181-1185.

Hu, G., Dam-Johansen, K., Wedel, S., Hansen, J.P., 2007. Enhancement of the direct sulfation of limestone by alkali metal salts, calcium chloride, and hydrogen

chloride. Industrial & Engineering Chemistry Research 46(16), 5295-5303.

Hu, G.L., Dam-Johansen, K., Wedel, S., Hansen, J.P., 2006. Review of the direct sulfation reaction of limestone. Progress in Energy and Combustion Science 32(4), 386-407.

I. Ávila, F.E. Milioli, Crnkovic, P.M., 2005. A kinetics study on the sorption of SO_2 by limestone through thermogravimetry, 18th International Congress of Mechanical Engineering. Ouro Preto, Brazil.

Idrissi, M., Diouri, A., Damidot, D., Greneche, J.M., Talbi, M.A., Taibi, M., 2010. Characterisation of iron inclusion during the formation of calcium sulfoaluminate phase. Cement and Concrete Research 40(8), 1314-1319.

Ige, O.E., Olanrewaju, O.A., Duffy, K.J., Obiora, C., 2021. A review of the effectiveness of Life Cycle Assessment for gauging environmental impacts from cement production. Journal of Cleaner Production 324.

Ingo, G.M., Riccucci, C., Bultrini, G., Chiozzini, G., 2001. Correlation between the surface acid-base nature of solid metal oxides and temperature of $CaSO_4$ decomposition. Journal of Thermal Analysis and Calorimetry 66(1), 27-35.

Jeong, S., Lee, K.S., Keel, S.I., Yun, J.H., Kim, Y.J., Kim, S.S., 2015. Mechanisms of direct and in-direct sulfation of limestone. Fuel 161, 1-11.

Jørgensen, T.L., Livbjerg, H., Glarborg, P., 2007. Homogeneous and heterogeneously catalyzed oxidation of SO_2. Chemical Engineering Science 62(16), 4496-4499.

Juenger, M.C.G., Snellings, R., Bernal, S.A., 2019. Supplementary cementitious materials: New sources, characterization, and performance insights. Cement and Concrete Research 122, 257-273.

Kocaefe, D., Karman, D., Steward, F.R., 1985. Comparison of the sulfation rates of calcium, magnesium and zinc oxides with SO_2 and SO_3. The Canadian Journal of Chemical Engineering 63(6), 971-977.

Li, X., Xu, W., Wang, S., Tang, M., Shen, X., 2014. Effect of SO_3 and MgO on Portland cement clinker: Formation of clinker phases and alite polymorphism. Construction and Building Materials 58, 182-192.

Li, Y.R., Li, F., Qi, H.Y., 2012. Numerical and experimental investigation of the effects of impinging streams to enhance Ca-based sorbent capture of SO_2. Chemical Engineering Journal 204, 188-197.

Liu, F., Ross, M., Wang, S., 1995. Energy efficiency of China's cement industry. Energy 20(7), 669-681.

Liu, L., Shao, G.C., Gong, P., Wu, Z.W., Chu, J.M., Hu, Y.G., Wang, J.F., Wang, S., Zheng, C.H., Gao, X., De Geyter, N., Morent, R., 2022. Density functional theory studies on ortho-position adsorption of SO_3 at step sites of a CaO surface with SO_2 and CO_2. Fuel 310, 122174.

Liu, Q., Sun, Y., Sun, Y., 2013. Cause analysis and countermeasure of gypsum rain in coal-fired power plants. Journal of Environmental Protection 4(1B), 1-4.

Lv, T., Lu, K., Song, L.J., 2011. Analysis and settlement of gypsum rain issue in

778 the wet-type FGD. Advanced Materials Research 347-353, 3396-3399.
779 Ma, S.H., Snellings, R., Li, X.R., Shen, X.D., Scrivener, K.L., 2021. Alite-
780 ye'elimite clinker: Hydration kinetics, products and microstructure. Construction and
781 Building Materials 266, 121062.
782 Ma, X.L., Tan, H.B., Dong, F.Q., Yang, F.H., 2022. Influence of carbon and pyrite
783 on desulfurization behavior of red gypsum at high temperature. Journal of Sustainable
784 Metallurgy 8(1), 409-418.
785 Malaga-Starzec, K., Panas, I., Lindqvist, O., 2004. Model study of initial
786 adsorption of SO_2 on calcite and dolomite. Applied Surface Science 222(1), 82-88.
787 Miller, S.W., Hansen, J.P., 2004. Methods for reducing SO_2 emissions, IEEE-
788 IAS/PCA 2004 Cement Industry Technical Conference. pp. 79-92.
789 Mut, M.D.M.C., Norskov, L.K., Frandsen, F.J., Glarborg, P., Dam-Johansen, K.,
790 2015. Review: Circulation of inorganic elements in combustion of alternative fuels in
791 cement plants. Energy & Fuels 29(7), 4076-4099.
792 Padilla-Encinas, P., Palomo, A., Blanco-Varela, M.T., Fernández-Carrasco, L.,
793 Fernández-Jiménez, A., 2021. Monitoring early hydration of calcium sulfoaluminate
794 clinker. Construction and Building Materials 295, 123578.
795 Pan, D.P., Wu, H., Yang, L.J., 2017. Investigation on the relationship between the
796 fine particle emission and crystallization characteristics of gypsum during wet flue gas
797 desulfurization process. Journal of Environmental Sciences 55, 303-310.
798 Pei, J., Pan, Y., Wu, Q., 2023. Performance and mechanism of sub-ppm SO_2
799 adsorption on the alkali modified activated carbon under different humidity level.
800 Journal of Cleaner Production 382, 135400.
801 Peys, A., Isteri, V., Yliniemi, J., Yorkshire, A.S., Lemougna, P.N., Utton, C., Provis,
802 J.L., Snellings, R., Hanein, T., 2022. Sustainable iron-rich cements: Raw material
803 sources and binder types. Cement and Concrete Research 157, 106834.
804 Poullikkas, A., 2015. Review of design, operating, and financial considerations in
805 flue gas desulfurization systems. Energy Technology & Policy 2(1), 92-103.
806 Przepiorski, J., Czyzewski, A., Pietrzak, R., Toyoda, M., Morawski, A.W., 2013.
807 Porous carbon material containing CaO for acidic gas capture: Preparation and
808 properties. Journal of Hazardous Materials 263, 353-360.
809 Qiu, K.R., Lindqvist, O., 2000. Direct sulfation of limestone at elevated pressures.
810 Chemical Engineering Science 55(16), 3091-3100.
811 Qiu, L.M., Zou, K., Xu, G.T., 2013. Investigation on the sulfur state and phase
812 transformation of spent and regenerated S zorb sorbents using XPS and XRD. Applied
813 Surface Science 266, 230-234.
814 Rasmussen, M.H., 2012. Low SO_2 emission preheaters for cement production.
815 Technical University of Denmark.
816 Sasmaz, E., Wilcox, J., 2008. Mercury species and SO_2 adsorption on CaO(100).
817 The Journal of Physical Chemistry C 112(42), 16484-16490.
818 Shen, W.G., Liu, Y., Yan, B.L., Wang, J., He, P.T., Zhou, C.C., Huo, X.J., Zhang,
819 W.Z., Xu, G.L., Ding, Q.J., 2017. Cement industry of China: Driving force,

environment impact and sustainable development. Renewable & Sustainable Energy Reviews 75, 618-628.

Shi, W.X., Lin, C., Chen, W., Hong, J.L., Chang, J.C., Dong, Y., Zhang, Y.L., 2017. Environmental effect of current desulfurization technology on fly dust emission in China. Renewable & Sustainable Energy Reviews 72, 1-9.

Shi, Z.G., Ferreiro, S., Lothenbach, B., Geiker, M.R., Kunther, W., Kaufmann, J., Herfort, D., Skibsted, J., 2019. Sulfate resistance of calcined clay-limestone-Portland cements. Cement and Concrete Research 116, 238-251.

Simoni, M., Hanein, T., Duvallet, T.Y., Jewell, R.B., Provis, J.L., Kinoshita, H., 2021. Producing cement clinker assemblages in the system: CaO-SiO_2-Al_2O_3-SO_3-$CaCl_2$-MgO. Cement and Concrete Research 144, 106418.

Snellings, R., 2016. Assessing, understanding and unlocking supplementary cementitious materials. RILEM Technical Letters 1(0), 50-55.

Staněk, T., 2016. The influence of SO_3 and MgO on kinetics of alite formation. Procedia Engineering 151, 26-33.

Tullin, C., Ljungstroem, E., 1989. Reaction between calcium carbonate and sulfur dioxide. Energy & Fuels 3(3), 284-287.

Wang, X., Li, Y.J., Zhu, T.Y., Jing, P.F., Wang, J.S., 2015. Simulation of the heterogeneous semi-dry flue gas desulfurization in a pilot CFB riser using the two-fluid model. Chemical Engineering Journal 264, 479-486.

Wang, Z., Yang, W., Liu, H., Jin, H., Chen, H.Q., Su, K., Tu, Y.J., Wang, W.L., 2019. Thermochemical behavior of three sulfates ($CaSO_4$, K_2SO4 and Na_2SO_4) blended with cement raw materials (CaO-SiO_2-Al_2O_3-Fe_2O_3) at high temperature. Journal of Analytical and Applied Pyrolysis 142, 104617.

Wang, Z.Q., Hu, Y.J., Cheng, X.X., Ma, C.Y., 2018. Study of adsorption characteristics of calcium-based sorbents with SO_3. Energy Procedia 144, 43-49.

Wu, C., 2020. Catalytic oxidation of SO_2 via vanadium-based catalysts in simulated preheater environment and consequent effect on SO_2 capture by calcium-based desulfurizer. South China University of Technology. (In Chinese).

Xu, D., Cui, Y.S., Li, H., Yang, K., Xu, W., Chen, Y.X., 2015. On the future of Chinese cement industry. Cement and Concrete Research 78, 2-13.

Yu, Q.J., Chen, R., Zhang, T.S., Wei, J.X., 2020. Recent development of flue gas de-SO_2 and de-NO_x technology for cement industry. Bulletin of the Chinese Society 39, 2015-2032. (In Chinese).

Zhang, H.P., Zhang, R., Ni, Y.X., Chen, M., Sun, C.H., Dong, F.Q., 2022. SO_2 adsorption and conversion on pristine and defected calcite {104} surface: A density functional theory study. Applied Surface Science 596, 153575.

Zhang, T.S., Wu, C., Li, B., Wang, C., Chen, X.Z., Wei, J.X., Yu, Q.J., 2019a. Clarifying the decomposition process of pyrite and SO_2 release in the cyclone preheater of a dry rotary cement kiln system. Journal of Cleaner Production 241, 118422.

Zhang, T.S., Wu, C., Li, B., Wang, J.W., Ravat, R., Chen, X.Z., Wei, J.X., Yu, Q.J., 2019b. Linking the SO_2 emission of cement plants to the sulfur characteristics of their

862 limestones: A study of 80 NSP cement lines in China. Journal of Cleaner Production
863 220, 200-211.
864 Zhang, X.M., Song, X.F., Sun, Z., Li, P., Yu, J.G., 2013. Density functional theory
865 study on the mechanism of calcium sulfate reductive decomposition by methane. Fuel
866 110, 204-211.
867 Zhu, J.P., Chen, Y.X., Zhang, L., Guo, B.K., Fan, G.X., Guan, X.M., Zhao, R.Q.,
868 2021. Revealing the doping mechanism of barium in sulfoaluminate cement clinker
869 phases. Journal of Cleaner Production 295, 126405.

870